Received: 22 March 2021 | Accepted: 27 May 2021

DOI: 10.1111/bpa.12996

Brain Pathology

RESEARCH ARTICLE

Dysregulated protein phosphorylation: A determining condition in the continuum of brain aging and Alzheimer's disease

Isidro Ferrer[1,2,3] | **Pol Andrés-Benito**[1,2,3] | **Karina Ausín**[4] | **Reinald Pamplona**[5] | **José Antonio del Rio**[6,7] | **Joaquín Fernández-Irigoyen**[4] | **Enrique Santamaría**[4]

[1]Department of Pathology and Experimental Therapeutics, University of Barcelona, Hospitalet de Llobregat, Spain

[2]CIBERNED (Network Centre of Biomedical Research of Neurodegenerative Diseases), Institute of Health Carlos III, Hospitalet de Llobregat, Spain

[3]Bellvitge University Hospital, Bellvitge Biomedical Research Institute (IDIBELL, Hospitalet de Llobregat, Spain

[4]Clinical Neuroproteomics Unit, Proteomics Platform, Proteored-ISCIII, Navarrabiomed, Complejo Hospitalario de Navarra (CHN), Universidad Pública de Navarra (UPNA, IdiSNA, Pamplona, Spain

[5]Department of Experimental Medicine, University of Lleida-Biomedical Research Institute of Lleida (UdL-IRBLleida, Lleida, Spain

[6]Molecular and Cellular Neurobiotechnology, Institute of Bioengineering of Catalonia (IBEC), Barcelona Institute for Science and Technology, Science Park Barcelona (PCB, Barcelona, Spain

[7]Department of Cell Biology, Physiology and Immunology, Faculty of Biology, University of Barcelona, Barcelona, Spain

Correspondence
Isidro Ferrer, Department of Pathology and Experimental Therapeutics, University of Barcelona, Feixa Llarga sn, 08907 Hospitalet de Llobregat, Barcelona, Spain.
Email: 8082ifa@gmail.com

Enrique Santamaría, Clinical Neuroproteomics Unit, Proteomics Platform, Proteored-ISCIII, Navarrabiomed, Complejo Hospitalario de Navarra (CHN), Universidad Pública de Navarra (UPNA), IdiSNA, Pamplona, Spain.
Email: enrique.santamaria.martinez@navarra.es

Funding information
The Proteomics Platform of Navarrabiomed is a member of Proteored (PRB3-ISCIII). The project leading to these results has received funding from "La Caixa" Banking Foundation under the project HR18-00452 to IF; it was also supported by the Ministry of Economy and Competitiveness, Institute of Health Carlos III (ISCIII) (co-funded by European Regional Development Fund, ERDF, a way to build Europe): FISPI17/000809 to IF; co-financed by ERDF under the program Interreg Poctefa: RedPrion 148/16 to IF; and the Intra-CIBERNED 2019 collaborative project to IF and JADR. We thank CERCA Programme/Generalitat de Catalunya for institutional support. We also thank CIBERNED (Instituto de Salud Carlos III: ISCIII), Ministry of Economy and Competitiveness for institutional backing. The Proteomics

Abstract

Tau hyperphosphorylation is the first step of neurofibrillary tangle (NFT) formation. In the present study, samples of the entorhinal cortex (EC) and frontal cortex area 8 (FC) of cases with NFT pathology classified as stages I–II, III–IV, and V–VI without comorbidities, and of middle-aged (MA) individuals with no NFT pathology, were analyzed by conventional label-free and SWATH-MS (sequential window acquisition of all theoretical fragment ion spectra mass spectrometry) to assess the (phospho)proteomes. The total number of identified dysregulated phosphoproteins was 214 in the EC, 65 of which were dysregulated at the first stages (I–II) of NFT pathology; 167 phosphoproteins were dysregulated in the FC, 81 of them at stages I–II of NFT pathology. A large percentage of dysregulated phosphoproteins were identified in the two regions and at different stages of NFT progression. The main group of dysregulated phosphoproteins was made up of components of the membranes, cytoskeleton, synapses, proteins linked to membrane transport and ion channels, and kinases. The present results show abnormal phosphorylation of proteins at the first stages of NFT pathology in the elderly (in individuals clinically considered representative of normal aging) and sporadic Alzheimer's disease (sAD). Dysregulated protein phosphorylation in the FC precedes the formation of NFTs and SPs. The most active period of dysregulated phosphorylation is at stages III–IV when a subpopulation of individuals might be clinically categorized as suffering from mild cognitive impairment which is a preceding determinant stage

Platform of Navarrabiomed is supported by grant PT17/0019/009 to JFI, of the PE I + D+I 2013-2016 funded by ISCIII and FEDER. Part of this work was funded by a grant from the Spanish Ministry of Science Innovation and Universities (Ref. PID2019-110356RB-I00) to JFI and ES, and the Department of Economic and Business Development from the Government of Navarra (Ref. 0011-1411-2020-000028) to ES

in the progression to dementia. Altered phosphorylation of selected proteins, carried out by activation of several kinases, may alter membrane and cytoskeletal functions, among them synaptic transmission and membrane/cytoskeleton signaling. Besides their implications in sAD, the present observations suggest a molecular substrate for "benign" cognitive deterioration in "normal" brain aging.

KEYWORDS
(phospho)proteomics, Alzheimer's disease, brain aging, cytoskeleton, kinases, membranes, protein phosphorylation, synapses, tau

1 | INTRODUCTION

Sporadic Alzheimer's disease (sAD) is a progressive disorder characterized by the presence of neurofibrillary tangles (NFTs) and senile plaques (SPs) distributed with a distinctive pattern throughout the brain in old age; however, the first NFTs, although few in number, may appear in young adulthood or even before (1). The main constituent of NFTs in sAD is a combination of all six 3R and 4R hyper-phosphorylated brain tau isoforms (2, 3). Tau pathology is now widely accepted as key in the pathogenesis of AD and other tauopathies (4–7). The study of consecutive series of the human population recognizes several stages of NFT pathology involving selected nuclei of the telencephalon and the brainstem, and increasing with age (8-10). Most individuals with NFT pathology restricted to the transentorhinal and entorhinal cortices and part of the hippocampus (first stages: stages I–II) are cognitively normal; cases at middle stages (stages III–IV), in which there is the involvement of the hippocampus and limbic system, may not suffer any apparent cognitive defect or suffer only mild cognitive impairment (MCI), often categorized as preclinical AD (11); cases at stages V–VI (advanced stages) in which almost all the telencephalon and basal ganglia are filled with NFTs suffer from dementia and they are categorized as sAD (12). About 85% of individuals aged 65 have NFT pathology, at least restricted to stages I–III (1, 13–15); only about 5% of them have dementia. The majority of individuals at stages I–II and almost half of those at stage III do not have SPs or β-amyloid deposits (13, 15). Increased numbers of SPs are common accompanying stage III–IV onwards. All cases with clinically and neuropathologically diagnosed sAD have NFTs stages V–VI and SPs; dementia of Alzheimer's type accounts for about 25%–30% of the population at the age of 85 years. In contrast, dementia with only tangles is exceptional. Therefore, sAD is an age-related continuum with variable timing of progression and strong individual variability, probably due to several genetic and environmental factors, and which starts as a slow, silent state for decades in the majority of individuals, but may progress to cognitive impairment in some elderly individuals, and then convert to dementia in relatively few of them (15-18). Recently, primary age-related tauopathy (PART) has been proposed to categorize a subpopulation of individuals with normal cognition or with mild cognitive impairment showing NFT pathology at stages I–IV of Braak and no SPs (19). Yet PART can also be interpreted within the spectrum of AD in cases with a particular genetic background characterized by a lower prevalence of *APOE e4*, *PTK2B*, *BIN1*, and *CR1* genes, and higher prevalence of APOE e2 (20-22).

The presence of a few NFTs and SPs in the medial temporal cortex, and NFTs in selected nuclei of the brainstem, is considered normal aging in clinical terms in any individual in his/her sixties having tolerable difficulties retrieving names and numbers, some degree of memory loss, and perhaps mild symptoms of depression.

The general hypothesis of the present study is that (a) widespread molecular alterations precede, participate in, and progress in parallel to the formation of NFTs and SPs in sAD and that tau phosphorylation is one, albeit a crucial one, of the many abnormally phosphorylated proteins in brain aging and sAD; (b) abnormal protein phosphorylation is determining in the dysfunction of numerous molecular pathways in brain aging and sAD. Pioneering studies have identified a few abnormally phosphorylated proteins in the hippocampus and cerebral cortex in small numbers of cases with AD compared with controls (23-27). Using more accurate methods, large numbers of dysregulated phosphoproteins have been identified in the frontal cortex in sAD cases compared with controls (28-30). However, we lack information about the alterations occurring at the first stages of NFT pathology (stages I–II) compared with the changes occurring at middle and advanced stages of disease progression.

To verify our hypothesis, the following objectives were decided upon: (1) identify abnormally phosphorylated proteins in two regions, the entorhinal cortex (EC) and frontal cortex area 8 (FC), differentially affected in aging and sAD; (2) learn whether abnormal protein phosphorylation develops at the first stages of NFT pathology without SPs in the FC in which the appearance of NFTs would be expected several years later; (3)

identify the principal groups of abnormally phosphorylated proteins in terms of cell localization and function in aging and sAD; (4) infer from the obtained data which neuronal functions may be altered at the first and middle NFT stages; and (5) point to putative alterations connecting altered protein phosphorylation and β-amyloid production.

Conventional label-free- and SWATH-MS (Sequential window acquisition of all theoretical fragment ion spectra mass spectrometry) were used to assess the (phospho)proteomes across NFT staging in the EC and FC of pure cases with NFT pathology classified as stages I–II, III–IV, and V–VI without co-morbidities and associated pathologies, and middle-aged (MA) individuals with no NFT pathology. Validation of a subgroup of proteins was carried out using immunohistochemistry and double-labeling immunofluorescence and confocal microscopy.

2 | MATERIAL AND METHODS

2.1 | Tissue samples

Post-mortem samples were obtained from the Institute of Neuropathology HUB-ICO-IDIBELL Biobank following the guidelines of Spanish legislation on this matter and the approval of the local ethics committee (CEIC) of Bellvitge University Hospital. The post-mortem interval between death and tissue processing was between 3 h and 11 h 15 min. One hemisphere was immediately cut in coronal sections, 1-cm thick, and selected areas of the encephalon were rapidly dissected, frozen on metal plates over dry ice, placed in individual air-tight plastic bags, numbered with water-resistant ink, and stored at −80℃ until used for biochemical studies. The other hemisphere was fixed by immersion in 4% buffered formalin for 3 weeks for morphologic study. Transversal sections of the spinal cord were alternatively frozen at −80℃ or fixed by immersion in 4% buffered formalin. The neuropathological study was carried out on paraffin sections of twenty-five selected regions of the cerebrum, cerebellum, brain stem, and spinal cord which were stained with hematoxylin and eosin, Klüver-Barrera, and periodic acid Schiff, or processed for immunohistochemistry with anti-β-amyloid, phospho-tau (clone AT8), α-synuclein, αB-crystallin, TDP-43, TDP-43-P, ubiquitin, p62, glial fibrillary acidic protein, CD68, and IBA1 antibodies (31).

Pathological cases (n = 15) were those having NFT Braak stages I–II (n = 5; 3 male, 2 women, 68.8 ± 10.9 years), III–IV (n = 5; 4 male, 1 female, 77.2 ± 5.7 years), and V–VI (n = 5; 81 ± 7.5 years). Cases with associated pathology including other tauopathies, α-synucleinopathy, TDP-43 proteinopathy, other neurodegenerative diseases, vascular diseases, and neoplastic diseases affecting the nervous system were excluded. Patients with arterial hypertension, type II diabetes, morbid obesity, hyperlipidemia, hepatic failure, renal failure, respiratory insufficiency, metabolic syndromes, and prolonged agonal states such as those occurring in intensive care units were eliminated. Cases with infectious, inflammatory, or autoimmune diseases, either systemic or limited to the nervous system, were not included. Middle-aged (MA) control cases (n = 9; 5 men, 4 women; 58.8 ± 12.3 years) had not suffered from neurologic or psychiatric diseases and did not have abnormalities in the neuropathological examination including the absence of NFTs.

Table 1 summarizes the characteristics of cases used in this series. NFT pathology was categorized according to the staging of Braak and Braak (8) modified for paraffin sections (32), β-amyloid deposits according to Thal phases (33), and CERAD scores according to the National Institute on Aging-Alzheimer's Association guidelines for the neuropathologic assessment of Alzheimer's disease (34, 35). Cases 12 and 14, which were categorized as phase A1 of Thal, had diffuse plaques in the frontal cortex but not in the entorhinal cortex.

Frozen samples of the frontal cortex (area 8) (FC) and entorhinal cortex (EC) were separately examined in parallel.

2.2 | (Phospho)proteomic analysis

EC and FC samples derived from MA and NFT Braak stages I–II, III–IV, and V–VI cases were homogenized in a lysis buffer containing 7 M urea, 2 M thiourea, and 50 mM DTT supplemented with protease and phosphatase inhibitors. The homogenates were spun down at 100,000 × *g* for 1 h at 15℃. Protein quantitation was performed with the Bradford assay kit (Bio-Rad). The EC and FC (phospho)proteomes and the corresponding proteomes across NFT staging were independently analyzed with conventional label-free- (36) and SWATH-MS (Sequential window acquisition of all theoretical fragment ion spectra mass spectrometry) (37), respectively. A 1.3-fold change cutoff and p-value lower than 0.05 were used for differential proteins and phosphopeptides. Proteins and phosphopeptides with ratios below the low range (0.77) were considered to be down-regulated, whereas those above the high range (1.3) were considered to be upregulated.

2.2.1 | Label-free phosphoproteomics

Six hundred micro grams of protein were used to obtain the phosphorylated fractions from EC and FC across NFT stages. For protein digestion, the reduction was performed with the addition of DTT to a final concentration of 10 mM and incubation at RT for 30 min. Subsequent alkylation with 30 mM (final concentration) iodoacetamide was performed for 30 min in the dark at

TABLE 1 Summary of cases used in this study

Case	Gender	Age	PMD	Amyloid /Thal phases	NFT/Braak stages	CERAD/neuritic plaque scores	Region	Clinical diagnosis
1	M	62	3 h 20 min	A0	B0	C0	EC	C
2	F	54	8 h	A0	B0	C0	EC	C
3	M	33	8 h 15 min	A0	B0	C0	EC	C
4	F	51	4	A0	B0	C0	EC	C
5	M	54	8 h 45 min	A0	B0	C0	EC, FC	C
6	F	65	4 h	A0	B0	C0	FC	C
7	M	62	3 h	A0	B0	C0	FC	C
8	M	70	13 h 40 min	A0	B0	C0	FC	C
9	F	79	7 h	A0	B0	C0	FC	C
10	M	63	3 h 50 min	A0	I–II (B1)	C0	EC, FC	N
11	M	64	8 h 35 min	A0	I–II (B1)	C0	EC, FC	N
12	M	86	5 h 35 min	A1	I–II (B1)	C0	EC, FC	N
13	F	55	9 h 30 min	A0	I–II (B1)	C0	EC, FC	N
14	F	76	5 h 45 min	A1	I–II (B1)	C0	EC, FC	N
15	M	85	4 h 45 min	2 (A1)	III–IV (B2)	C2	EC, FC	MCI
16	M	75	6 h 10 min	A1	III–IV (B2)	C1	EC, FC	N
17	M	77	11 h 15 min	2 (A1)	III–IV (B2)	C2	EC, FC	N
18	M	81	7 h 30 min	3 (A2)	III–IV (B2)	C2	EC, FC	MCI
19	F	68	4 h 45 min	2 (A1)	III–IV (B2)	C2	EC, FC	N
20	M	92	7 h 45 min	3 (A2)	V–VI (B3)	C3	EC, FC	A dementia
21	M	85	3 h 45 min	4 (A3)	V–VI (B3)	C3	EC, FC	A dementia
22	F	84	7 h 45 min	4 (A3)	V–VI (B3)	C3	EC, FC	A dementia
23	M	82	5 h	4 (A3)	V–VI (B3)	C3	EC, FC	A dementia
24	W	72	9 h 30 min	4 (A3)	V–VI (B3)	C3	EC, FC	A dementia

Note: Amyloid/Thal phases (1: deposits exclusive in neocortex, 2: plus allocortex, 3: plus diencephalic nuclei, striatum, and nuclei of the basal forebrain, 4: plus brainstem; modified NIA-AA: A0, A1, A2, A3, A4); NFT/Braak stages: Braak stages of neurofibrillary tangle pathology (modified B0, B1, B2, B3); CERAD/neuritic plaque scores (C0: none, C1: sparse, C2: moderate, C3: frequent).

Abbreviations: A dementia, Alzheimer's dementia; C, control; EC, entorhinal cortex; F, female; FC, frontal cortex area 8; M, male; MCI, mild cognitive impairment; N, cognitively normal; PMD, post-mortem delay.

room temperature. An additional reduction step was carried out with 30 mM DTT (final concentration), allowing the reaction to stand at room temperature for 30 min. The mixture was diluted to 0.6 M urea using MilliQ-water, and after the addition of trypsin (Promega) (enzyme: protein, 1:50 w/w), the sample was incubated at 37℃ for 16 h. Digestion was quenched by acidification (pH < 6) with acetic acid. After protein enzymatic cleavage, peptide cleaning was performed using Pierce™ Peptide Desalting Spin Columns (ThermoFisher). To obtain the phosphorylated peptide fractions, the High-Select™ TiO_2 Phosphopeptide Enrichment Kit (Thermo Scientific) was used according to the manufacturer's instructions. Phosphopeptide mixtures were separated by reversed-phase chromatography using an Eksigent NanoLC ultra 2D pump fitted with an Acclaim™ PepMap™ 100 C18 column (0.075 × 250 mm, particle size 3 μm; ThermoFisher). Samples were first loaded for concentration into an Acclaim™ PepMap™ 100 C18 trap column (0.1 × 20 mm, particle size 5 μm; ThermoFisher). Mobile phases were 100% water 0.1% formic acid (FA) (buffer A), and 100% acetonitrile 0.1% FA (buffer B). The column gradient was developed in a gradient from 2% B to 40% B in 120 min. The column was equilibrated in 95% B for 10 min and 2% B for 10 min. During the entire process, the precolumn was in line with the column, and flow was maintained all along the gradient at 300 nl/min. The eluting peptides were analyzed using a 5600 TripleTOF mass-spectrometer (Sciex). Information data acquisition was made with a survey scan performed in a mass range from 350 up to 1250 m/z in a scan time of 25 ms. The top 15 peaks were selected for fragmentation. The minimum accumulation time for MS/MS was set at 200 ms giving a total cycle time of 3.3 s. The produced ions were scanned in a mass range from 100 up to 1500 m/z and excluded for further fragmentation for 15 s. The raw MS/MS spectra searches were processed using the MaxQuant software (v 1.6.7.0) and searched against the Uniprot proteome reference for *Homo sapiens* (Proteome ID: UP000005640_9606, February 2019). The parameters used were as follows: initial maximum precursor (15 ppm) fragment mass deviations (20 ppm); fixed

modification [Carbamidomethyl (C)]; variable modification [Oxidation (M)]; Acetyl [Protein N-terminal; Deamidation (N); Gln > puroGlu; Phospho (STY)]; enzyme (trypsin) with a maximum of 1 missed cleavage; minimum peptide length (7 amino acids); and false discovery rate (FDR) for PSM and protein identification (1%). Frequently observed laboratory contaminants were removed. The Perseus software (version 1.5.6.0) was used for statistical analysis and data visualization.

2.2.2 | SWATH-MS

For protein expression analysis, 2 independent pools of multiple human brain structures were used as input for the generation of the SWATH-MS essay library. To increase proteome coverage, in-solution and in-gel digestion workflows were applied. In the first case, protein material from each pooled sample was precipitated using methanol/chloroform extraction. The pellet was dissolved in 6 M urea, 100 mM Tris, pH 7.8. Protein digestion was performed as described above. The digestion mixture was dried in a SpeedVac, reconstituted with 110 μL 5 mM ammonium formate pH 10, and injected into an ÄKTA pure 25 system (GE Healthcare Life Sciences) with a high pH stable X-Terra RP18 column (C18; 1 mm × 150 mm; 5 μm) (Waters). Peptides were eluted with a mobile phase B (5 mM ammonium formate in 90% ACN at pH 10) of 30–70% linear gradient over 45 min (A, 5 mM ammonium formate in the water at pH 10; B, 5 mM ammonium formate in 90% ACN at pH 10). The UV signal was monitored at 215 nm. Fractions were collected and evaporated in a vacuum. Neighboring fractions with low signal intensity were subsequently pooled to generate fractions with similar peptide content. For the second digestion protocol, protein extracts (20 ug) were diluted in Laemmli sample buffer and loaded into a 1.5 mm thick polyacrylamide gel with a 4% stacking gel cast over a 12.5% resolving gel. The total gel was stained with Coomassie Brilliant Blue, and 12 equal slides from each pooled sample were excised from the gel and transferred into 1.5 ml Eppendorf LoBind tubes. Protein enzymatic cleavage was carried out with trypsin (Promega; 1:20, w/w) at 37℃ for 16 h as previously described (38). Purification and concentration of peptides were performed using C18 Zip Tip Solid Phase Extraction (Millipore). The peptides, recovered from in-gel and in-solution digestion processing, were reconstituted into a final concentration of 0.5 μg/μl of 2% ACN, 0.5% FA, 97.5% MilliQ-water before mass spectrometric analysis. MS/MS datasets for spectral library generation were acquired on a TripleTOF 5600+ mass spectrometer (Sciex) interfaced to the Eksigent nanoLC ultra 2D pump system (Sciex) as previously described. MS/MS data acquisition was performed using AnalystTF 1.7 (Sciex), and spectra files were processed through ProteinPilot v5.0 search engine (Sciex) using Paragon™ Algorithm (v.4.0.0.0) (39) for database search. To avoid using the same spectral evidence in more than one protein, the identified proteins were grouped based on MS/MS spectra with the Progroup™ Algorithm, regardless of the peptide sequence assigned. False discovery rate (FDR) was determined using a non-linear fitting method (40) and displayed results were those reporting a 1% Global FDR or better. Then, individual protein extracts from all sample sets (n = 40) were subjected to in-solution digestion, peptide purification, and reconstitution before mass spectrometric analysis as previously mentioned. For SWATH-MS-based experiments, the TripleTOF 5600+ instrument was configured as described by Gillet et al. (41). Using an isolation width of 16 Da (15 Da of optimal ion transmission efficiency and 1 Da for the window overlap), a set of 37 overlapping windows was constructed covering the mass range 450–1000 Da. In this way, 1 μl of each sample was loaded onto an Acclaim™ PepMap™ 100 C18 trap column (0.1 × 20 mm, particle size 5 μm; ThermoFisher) and desalted with 100% water 0.1% formic acid at 2 μl/min for 10 min. The peptides were loaded onto an Acclaim™ PepMap™ 100 C18 column (0.075 × 250 mm, particle size 3 μm; ThermoFisher) equilibrated in 2% acetonitrile 0.1% FA. Peptide elution was carried out with a linear gradient of 2 to 40% B in 120 min (mobile phases A: 100% water 0.1% formic acid (FA) and B: 100% acetonitrile 0.1% FA) at a flow rate of 300 nl/min. Eluted peptides were infused in the mass-spectrometer. The Triple TOF was operated in SWATH mode, in which a 0.050 s TOF MS scan from 350 to 1250 m/z was performed, followed by 0.080 s product ion scans from 230 to 1800 m/z on the 37 defined windows (3.05 s/cycle). The collision energy was set to optimum energy for a 2+ ion at the center of each SWATH block with a 15 eV collision energy spread. The resulting ProteinPilot group file from library generation was loaded into PeakView® (v2.1, Sciex), and peaks from SWATH runs were extracted with a peptide confidence threshold of 99% (Unused Score ≥1.3) and FDR lower than 1%. For this, the MS/MS spectra of the assigned peptides were extracted with ProteinPilot, and only the proteins that fulfilled the following criteria were validated: (1) peptide mass tolerance lower than 10 ppm, (2) 99% confidence level in peptide identification, and (3) complete b/y ions series found in the MS/MS spectrum. Only proteins quantified with at least two unique peptides were considered. The cellular localization and main functions of the differential proteins were retrieved from www.genecards.org; www.uniprot.org; www.ebi.ac.uk (InterPro); www.OMIM.org; www.ncbi.nlm.nih.org. All MS raw data and search result files have been deposited at the ProteomeXchange Consortium (http://proteomecentral.proteomexchange.org) via the PRIDE partner repository with the dataset identifiers PXD021645 (Reviewer account details: Username: reviewer_pxd021645@ebi.ac.uk; Password: ANBskoaI) and PXD021653 (Reviewer account details:

Username: reviewer_pxd021653@ebi.ac.uk; Password: kMAyoOkq).

2.2.3 | Bioinformatics

The identification of significantly dysregulated regulatory/metabolic pathways in EC and FC proteomic datasets was made using Metascape (42). Network analysis was performed by submitting the corresponding protein IDs to the STRING (Search Tool for the Retrieval of Interacting Genes) software (http://stringdb.org/) (43). Proteins are represented with nodes and all the edges were supported by at least one reference from the literature or canonical information stored in the STRING database. To minimize false positives as well as false negatives, only interactions tagged as "medium confidence" (>0.4) in STRING database were considered.

2.3 | Immunohistochemistry and double-labeling immunofluorescence and confocal microscopy

Formalin-fixed, paraffin-embedded 4 μm-thick tissue sections of the EC and FC were obtained with a sliding microtome. The sections were processed for immunohistochemistry. The sections were boiled in citrate buffer (20 min) to retrieve protein antigenicity. Endogenous peroxidases were blocked by incubation in 10% methanol–1% H_2O_2 solution (15 min) followed by 3% normal horse serum solution. Then the sections were incubated at 4℃ overnight with one of the primary antibodies listed in Table 2. Following incubation with the primary antibody, the sections were incubated with EnVision + system peroxidase (Dako, Agilent Technologies, Santa Clara, CA, USA) for 30 min at room temperature. The peroxidase reaction was visualized with diaminobenzidine and H_2O_2. Control of the immunostaining included omission of the primary antibody; no signal was obtained following incubation with only the secondary antibody.

For double-labeling immunofluorescence, the tissue sections were stained with a saturated solution of Sudan black B (Merck, Glostrup, DE) for 15 min to block the autofluorescence of lipofuscin granules present in cell bodies, and then rinsed in 70% ethanol and washed in distilled water. The sections were incubated at 4℃ overnight with combinations of primary antibodies AT8 and anti-p38 kinase P Thr180/Tyr182 or PKAα/β Thr197. After washing, the sections were incubated with Alexa488 and Alexa546 (1:400, Molecular Probes, Eugene, OR, USA) fluorescence secondary antibodies against the corresponding host species. Nuclei were stained with DRAQ5^{TM} (dilution 1:2000, BioStatus, Loughborough, UK). After washing, the sections were mounted in Immuno-Fluore mounting medium (ICN Biomedicals, Irvine, CA, USA), sealed, and dried overnight. Sections were examined with a Leica TCS-SL confocal microscope.

3 | RESULTS

To quantify region-dependent fluctuations on a proteome-wide scale, we performed an integrative analysis of the proteome and phosphoproteome across NFT stages in the EC and FC.

TABLE 2 Antibodies used

Antibody	Supplier	Reference	Species	Dilution hi
AT8	Innogenetics	clone AT-8	ms	1:50
Catenin β-P Ser45/Thr41	Cell Signaling	9565	rb	1:50
MAP2-P Thr1620/1623	Cell Signaling	4544	rb	1:1000
Adducin 1- (ADD1) P Ser726	Abcam	ab53093	rb	1:100
ADD1/ADD2- P Ser726/Ser713	Thermo-Fisher Invitrogen	PA5-36614	rb	1:100
p38-P Thr180/Tyr182	Cell Signaling	9211	rb	1:100
SAPK/JNK-P Thr183/Thr185	Cell Signaling	9251	rb	1:50
PAK1-P Ser199/Ser204	Merck-Sigma-Aldrich	09-258	rb	1:100
NFL-P Ser473 (clone 4F8)	Merck-Sigma-Aldrich	MABN2431	ms	1:100
NFH	Abcam	Ab8135	rb	1:1000
NFH (200 kDa) RT97	Merck-Sigma-Aldrich	Mab5262	ms	1:50
NFM (160 kDa) BF10	Boehringer	1178687	ms	1:50
PAK1-P Ser199/Ser204	Merck-Sigma-Aldrich	09-258	rb	1:100

Abbreviations: MAP2, microtubule-associated protein 2; NFH, NF high molecular weight; NFL, neurofilament low molecular weight; NFM, NF medium molecular weight; p38, p38 kinase; PKAα/β, protein kinase A α/β; SAPK/JNK, Stress-activated protein kinase (*SAPK)/Jun amino-terminal kinase (JNK).*

3.1 | Proteome and phosphoproteome dynamics in the EC

Heatmaps of proteomes and phosphoproteomes showed marked differences in the EC between MA and the different stages of NFT pathology. The total number of different identified dysregulated proteins was 230 (57 at stage I–II, 89 at stage III–IV, and 136 at stage V–VI). The total number of different identified dysregulated phosphoproteins was 214, corresponding to 65 at stages I–II, 135 at stages III–IV, and 118 at stages V–VI (total number of phosphosites 83, 225, and 195, respectively) (Figure 1A). Some of them were common to different stages. Direction of dysregulation (hyper- or hypophosphorylation compared to MA) was variable depending on the stage, with no apparent predetermined patterns. Some phosphoproteins showed more than one phosphorylation site; the direction of phosphorylation (hyper- or hyporegulation) was independent of the phosphorylation site (Table S1).

Comparison between total dysregulated proteins and dysregulated phosphoproteins showed 42 dysregulated phosphoproteins not accompanied by concomitant altered expression of their total corresponding protein levels, 23 not quantified, and 0 overlapping at stages I–II (total phosphoproteins 65); 93 dysregulated phosphoproteins not accompanied by concomitant altered expression of their corresponding total protein levels, 42 not quantified, and 3 phosphoproteins with altered steady-state protein levels at stages III–IV (total phosphoproteins 135); and 83 dysregulated phosphoproteins not accompanied by concomitant altered expression of their total corresponding protein level, 35 not quantified, and 7 phosphoproteins with altered levels of the total protein at stages V–VI (total phosphoproteins 118) (Table S2).

Comparative analysis of different stages revealed 22 phosphoproteins common to the three stages, 40 phosphoproteins common to stages V–VI and III–IV, 10 phosphoproteins common to stages V–VI and I–II, and 10 phosphoproteins common to stages III–IV and I–II (Figure 1B). A comparative diagram of common and stage-specific dysregulated proteins is shown in the same figure where no overlap is seen between dysregulated proteins and dysregulated phosphoproteins at the different NFT stages.

To characterize in detail the entorhinal proteostatic modulation across NFT stages, differential proteomic and phosphoproteomic datasets were merged, and then functionally analyzed across specific biological functions. The phosphoprotein overlap previously described was also accompanied by a considerable overlap in the significantly enriched GO terms across NFT stages associated with cell morphogenesis involved in differentiation, synapse organization, vesicle-mediated transport, nervous system development, chemical synaptic transmission, neuronal systems, response to wounding, regulation of membrane potential, synaptic vesicle cycle, ECM-receptor interaction, regulated exocytosis, protein localization to membrane, regulation of vesicle-mediated transport, regulation of system process, dendritic development, cellular response to external stimuli, microtubule cytoskeleton organization, and regulation of cell morphogenesis (Table S3). The number of disrupted pathways increased with disease progression when considering the sum of disrupted pathways across NFT staging, disrupted pathways common to stages III–IV and V–VI, and disrupted pathways at stages V–VI. Importantly, many disrupted pathways were common to the first (I–II), middle (III–IV), and advanced (V–VI) stages, thus indicating a continuity of altered putative function derived from aberrant proteostasis starting at the first stages of the biological process (Figure 2).

3.2 | Proteome and phosphoproteome dynamics in the FC

The total number of identified dysregulated proteins was 82 (23 at stage I–II, 31 at stage III–IV, and 37 at stage V–VI) compared with MA. The total number of identified dysregulated phosphoproteins was 167, corresponding to 81 at stages I–II, 92 at stages III–IV, and 79 at stages V–VI (total number of phosphosites 100, 129, and 101, respectively) (Figure 3A; Table S2). The direction of dysregulation (hyper- or hypophosphorylation compared to MA) was variable depending on the stage and region with no apparent predetermined patterns (Table S4).

Comparison between total dysregulated proteins and dysregulated phosphoproteins showed 56 dysregulated phosphoproteins without concomitant variation in total protein levels at stages I–II, 61 at stages III–IV, and 55 at stages V–VI; not quantified were 25, 31, and 24 at stages I–II, III–IV, and V–VI, respectively (Table S2).

The comparative analysis between different stages revealed 21 phosphoproteins common to the three stages, 14 phosphoproteins common to stages V–VI and III–IV, 14 (phospho)proteins common to stages V–VI and III–IV, 14 (phospho)proteins common to stages V–VI and I–II, and 15 phosphoproteins common to stages III–IV and I–II (Figure 3B). No overlap was observed between dysregulated proteins and dysregulated phosphoproteins at the different NFT stages.

As observed in the EC, a functional overlap was also detected in the FC during NFT staging progression, revealing alterations in actin filament-based process, cellular morphogenesis, synapse organization, axon guidance, cell junction organization, maintenance of cell polarity, neurexins, and neuroligins, negative regulation of cellular components organization, semaphorin interactions, chemical synaptic transmission, neuronal systems, muscle system process, positive regulation of

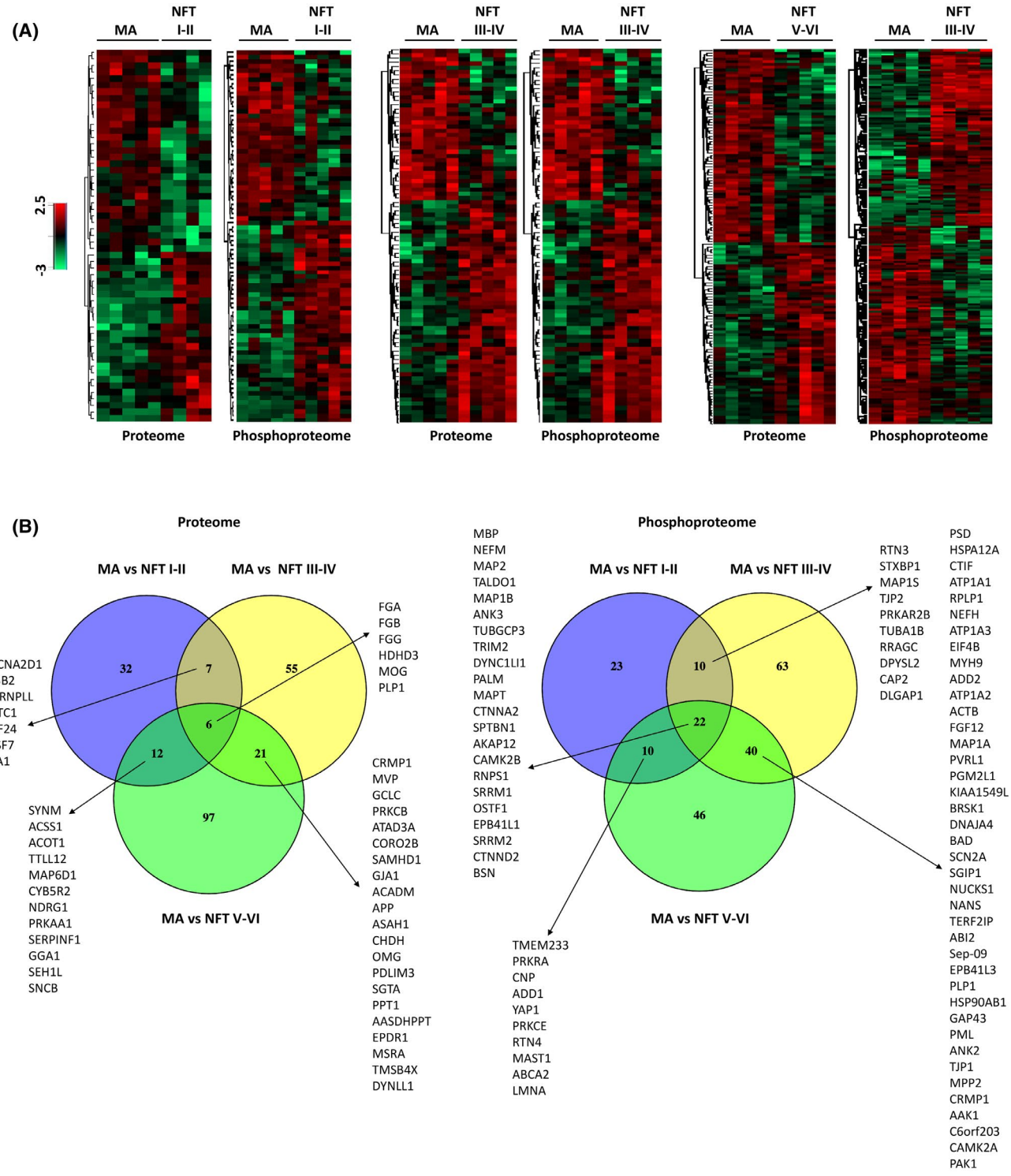

FIGURE 1 (A) Heatmap representation showing both clustering and the degree of change for the differentially expressed (phospho) proteins in NFT I–II (left), NFT III–IV (middle), and NFT V–VI (right) at the EC. (B) Common and unique differential EC (phospho)proteins across NFT staging. Venn diagrams show the overlap between differential EC proteins (left) and (phospho)proteins (right) across NFT staging. Gene names are indicated for the corresponding overlapping areas

cellular components movements, apoptosis, dendrite development, transport along the microtubule, positive regulation of hydrolase activity, establishment of organelle localization, and actomyosin structure organization (Table S5). The heatmap of common and stage-specific altered functions in the FC across NFT staging is shown in Figure 4. The figure also serves to highlight how several functional pathways are altered at the first and middle stages of the process while many are altered at stages I–II, III–IV, and V–VI.

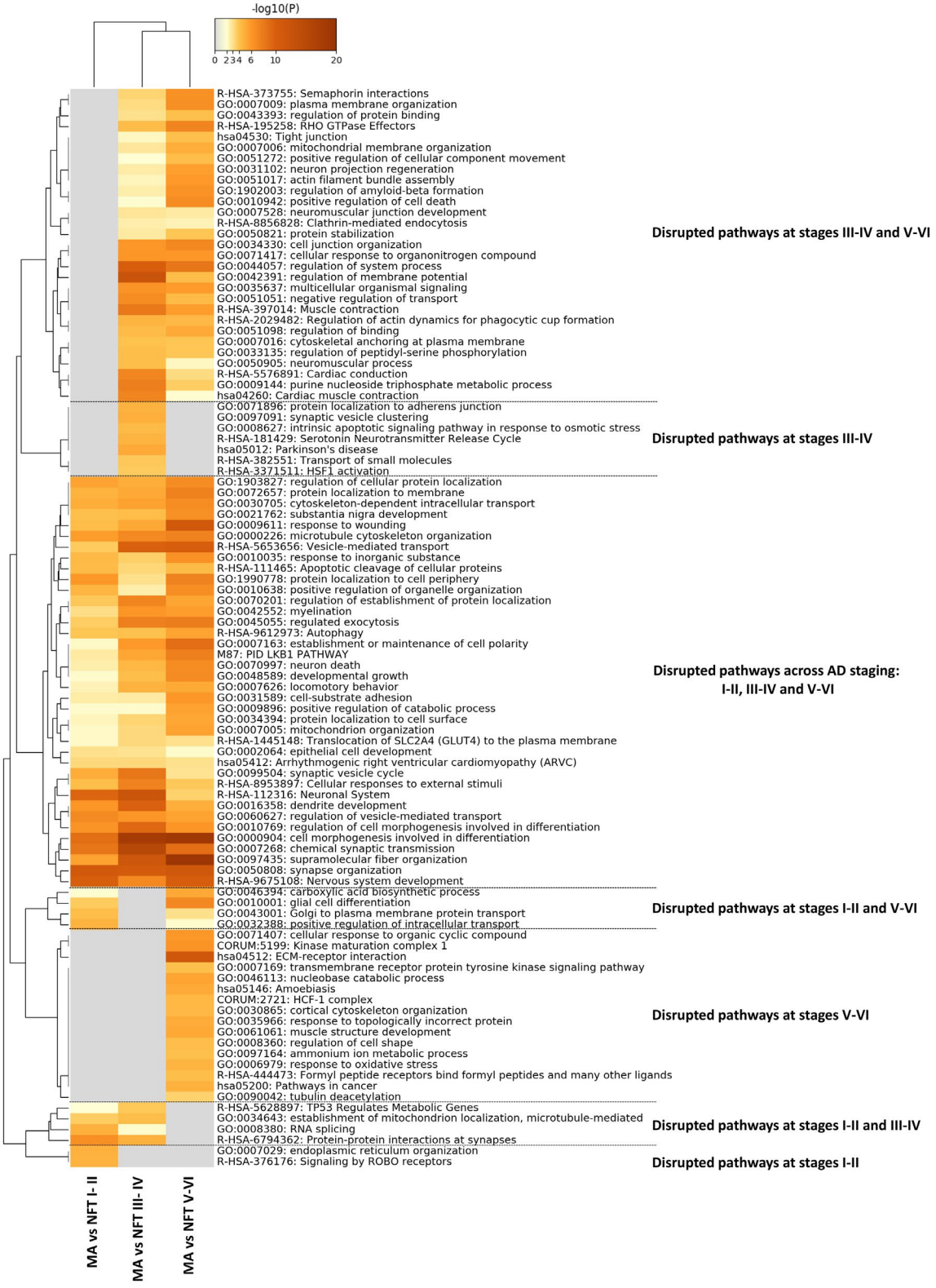

FIGURE 2 Enriched ontology clusters in the EC differential (phospho)proteomes during NFT progression. After identification of all statistically enriched terms, cumulative hypergeometric p-values and enrichment factors were calculated and used for filtering. The remaining significant terms were then hierarchically clustered into a tree based on Kappa-statistical similarities among their gene memberships. Then, a 0.3 kappa score was applied as the threshold to cast the tree into term clusters. The term with the best p-value within each cluster was selected as its representative term and displayed in a dendrogram. The heat map cells are colored for their p-values; grey cells indicate a lack of enrichment

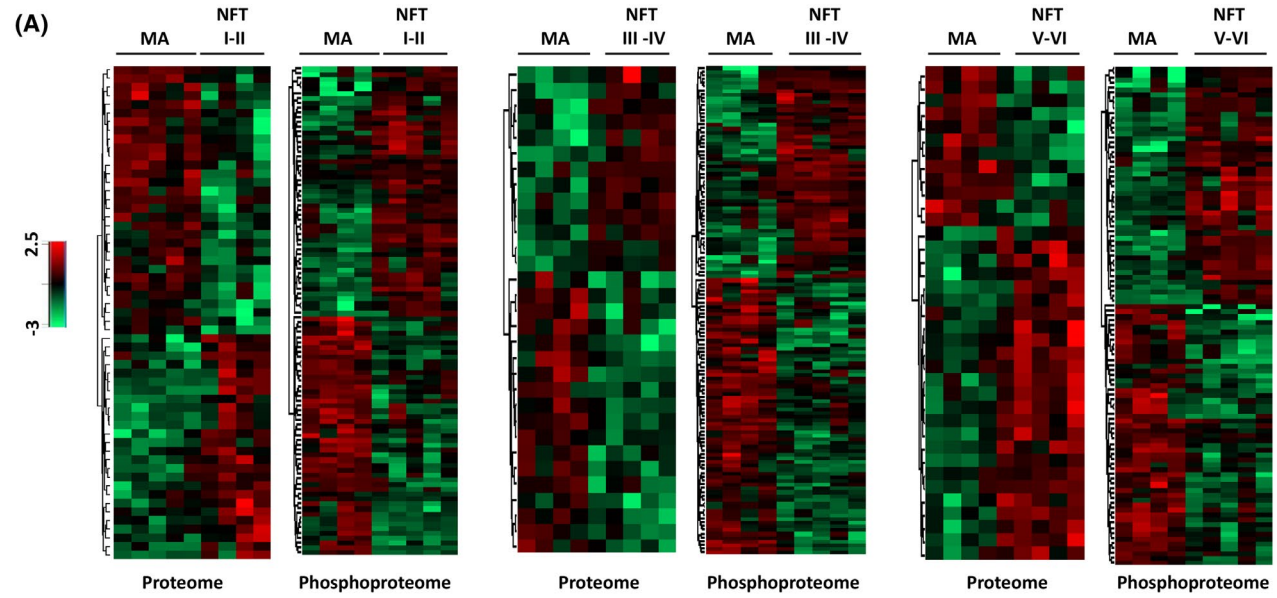

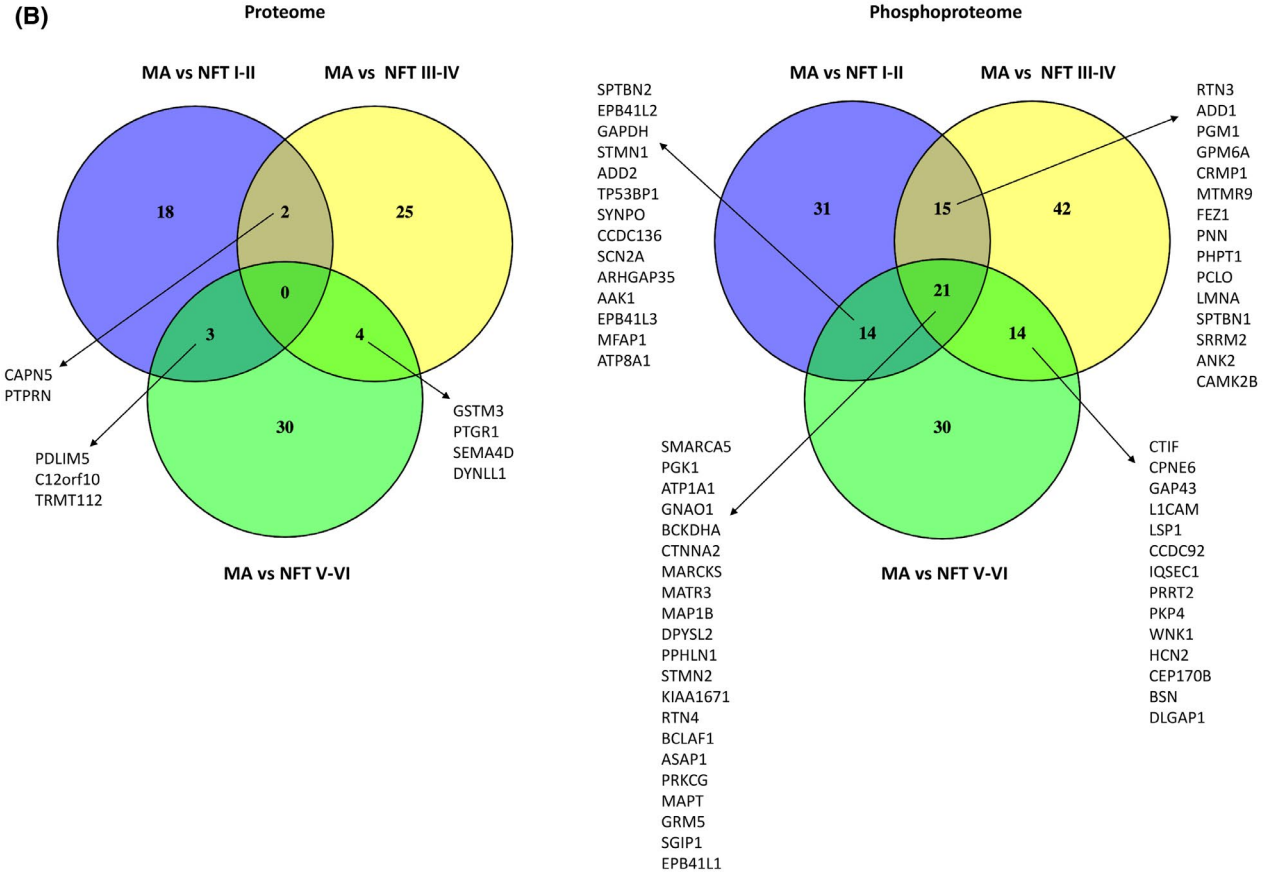

FIGURE 3 (A) Heatmap representation showing both clustering and the degree of change for the differentially expressed (phospho) proteins in NFT stages I–II (left), NFT III–IV (middle), and NFT V–VI (right) in the FC. (B) Common and unique differential FC (phospho) proteins across NFT staging. Venn diagrams show the overlap between differential FC proteins (left) and phosphoproteins (right) during AD progression. Gene names are indicated for the corresponding overlapping areas

FIGURE 4 Enriched ontology clusters in FC differential (phospho)proteomes during AD progression. After identification of all statistically enriched terms, cumulative hypergeometric p-values and enrichment factors were calculated and used for filtering. The remaining significant terms were then hierarchically clustered into a tree based on Kappa-statistical similarities among their gene memberships. Then, a 0.3 kappa score was applied as the threshold to cast the tree into term clusters. The term with the best p-value within each cluster was selected as its representative term and displayed in a dendrogram. The heat map cells are colored for their p-values; grey cells indicate the lack of enrichment

3.3 | Individualized analysis of differentially phosphorylated proteins expressed in the EC and FC

To better characterize the relevance of differentially phosphorylated proteins and their implication in the pathobiology of sAD, phosphoproteins were manually categorized into several groups one by one according to their localization and function. Cytoskeletal and membrane proteins, proteins of the synapses and dense core vesicles, myelin proteins, and proteins linked to membrane transport and ion channels accounted for 144 differentially phosphorylated proteins. Their symbols, full names, main functions, and presence in the EC and FC at different stages of NFT pathology are summarized in Table 3.

The largest group of dysregulated phosphoproteins was made up of cytoskeletal and membrane proteins (n = 91) which included proteins of microfilaments, actin-binding proteins, intermediate filaments of neurons and glial cells, proteins associated with microtubules, integral membrane proteins, and peripheral membrane proteins. The EC and FC shared thirty-one proteins abnormally phosphorylated. Thirty-five proteins were identified as differentially phosphorylated in at least two stages in the EC and 28 proteins in the FC in AD when compared with MA. Twenty-three dysregulated phosphoproteins were identified in only one region or one stage of the disease. A second group was made up of phosphoproteins of the synapses and dense core vesicles (n = 21). This classification was instrumental as some membrane proteins also participated in the structure of the synapses, and several synaptic proteins were considered plasma membrane proteins. Six proteins were identified in both the EC and FC. Four proteins were differentially phosphorylated in two stages of AD in the EC, and five in the FC. Twelve proteins were identified in only one region or one stage of the disease. The third group included a few myelin-associated phosphoproteins (myelin basic protein, myelin proteolipid protein, and 2′,3′-cyclic nucleotide 3′ phosphodiesterase). The fourth group was represented by phosphoproteins linked to membrane transport and ion channels (n = 28). Eight dysregulated phosphorylated proteins were common to the EC and FC: Seven phosphoproteins were altered in two stages in AD in the EC, and twelve in the FC. Ten dysregulated phosphoproteins were identified in only one region or one stage of the disease.

Other dysregulated phosphoproteins were categorized as kinases, proteins linked to DNA or protein deacetylation, proteins linked to gene transcription and protein synthesis, heat-shock proteins, members of the ubiquitin-proteasome system (UPS), and proteins involved in energy metabolism. The list included 77 phosphoproteins. Their symbols, full names, main functions, and occurrence in the EC and FC at different stages of NFT are summarized in Table 4. Twenty-one kinases with dysregulated phosphorylation were identified. Five (phospho)proteins linked to DNA were dysregulated in the EC, all of them at stages III–IV and/or V–VI. Two were dysregulated in the FC. Another major group was composed of 31 dysregulated phosphoproteins linked to gene transcription and protein synthesis. Eighteen phosphoproteins were detected in the EC, eighteen in the FC, and thirteen in at least two stages in the FC or EC. Dysregulated phosphorylation of heat-shock proteins was found in the EC at stages III–IV and V–VI. Seven phosphoproteins involved in the UPS were abnormally regulated, five of them only in the EC, and only one in two stages. Only two phosphoproteins linked to the UPS were abnormally regulated in the FC. Finally, the distribution of abnormally regulated phosphoproteins linked to energy metabolism was largely region-dependent. Of the total 14 dysregulated phosphoproteins, only three were common to the EC and FC. Other dysregulated phosphoproteins were heterogeneous and identified in only one stage and in one region (Tables S1 and S4).

3.4 | Dysregulated phosphoproteins at the first stages of NFT pathology

Several phosphoproteins linked to the structure and function of cell membranes, cytoskeleton, and synapses were dysregulated at the first stages of NFT pathology in the EC and FC. Thirty-six phosphoproteins were dysregulated in the EC at stage I–II in comparison with MA individuals. Forty-seven phosphoproteins were abnormally regulated in the FC at stage I–II (Table 3).

Dysregulated phosphorylation of proteins categorized as kinases, proteins linked to DNA or protein deacetylation, proteins linked to gene transcription and protein synthesis, and proteins involved in energy metabolism also occurred in the EC and FC at the first stages of NFT pathology. Nineteen phosphoproteins were dysregulated in the EC at stages I–II compared with MA. Twenty-five dysregulated phosphoproteins were identified in the FC at stages I–II (Table 4).

3.5 | Interactions of dysregulated phosphoproteins linked to the structure and function of cell membranes, synapses, and cytoskeleton

The interactions of dysregulated phosphoproteins in the EC and FC at different stages of NFT pathology are summarized in Figure 5. Protein tau interacts with several proteins but many others have no direct interactions with tau, thus suggesting that the phosphorylation of a particular protein does not necessarily depend on the phosphorylation state of tau. As detailed above, dysregulated protein phosphorylation started at the first stages of NFT pathology. The greater number of different

TABLE 3 Dysregulated cytoskeletal, synaptic, and membrane phosphoproteins in the entorhinal cortex (EC) and frontal cortex area 8 (FC) at different stages of NFT pathology (stages I–II, III–IV, and V–VI of Braak) compared with middle-aged individuals

			EC I–II	EC III–IV	EC V–VI	FC I–II	FC III–IV	FC V–VI
Cytoskeleton and membranes								
ACTB	Actin cytoplasmic 1; actin β	Main component of microfilaments		1↓	1↓		1↓	
NEFM	Neurofilament medium polipeptide	Intermediate neurofilaments	1↓ 2↑	3↓ 1↑	3↓		1↓ 1↑	
NEFH	Neurofilament heavy polipeptide			2↓	2↓			
INA	α-internexin	Intermediate neurofilament enriched in frontal cortex					1↓	
TUBA1B	Tubulin α-1B chain	Components of microtubules	1↑	1↑				
TUBGCP3	γ-tubulin complex component 3		1↑	1↑	1↑			
TPPP	Tubulin polimerization promoting protein			1↑				
MAP1A	Microtubule-associated protein 1A			3↑	2↓	1↑		
MAP1B	Microtubule-associated protein 1B		3↓ 1↑	12↓ 5↑	9↓ 1↑	2↑	5↓ 3↑	3
MAP2	Microtubule associated protein 2		2↑	1↓ 6↑	2↓ 5↑		1↑	
MAPT	Microtubule associated protein tau		3↓	2↓ 5↑	1↓ 23↑	3↑	1↓ 1↑	4↑
MAP1S	Microtubule associated 1S		1↓	1↓				
DYNC1LI1	Cytoplasmic dynein 1 light intermediate chain 1	Dyneins transport cargos along microtubules and are responsible of retrograde axonal transport	1↓ 1↑	1↑	1↑			1↓ 1↑
DYNC1LI2	Cytoplasmic dynein 1 light intermediate chain 2			1↓				
DYNC 1/1	Cytoplasmic dynein intermediate chain				1↓			
KIF21A	Kinesin-like protein KIF21A	Kinesins facilitate anterograde axonal transport		1↓				
NFASC	Neurofascin	IGcam organization axon initial segment		1↓		1↓		
SEPTIN9	Septin9	Growth and stability of axons, dendrites and synapses		1↑	1↑		1↓	
SEPTIC4	Septin4	GTPase activity; cytoskeleton dependent cytokinesis					2↑	
PLEC	Plectin	Binding cytoskeleton			3↑			
DPYSL2	Dydropyrimidinase-related protein	Member of the collapsing response mediator protein family; promotes microtubule assembly	1↓	2↓ 1↑		3↓ 1↑	2↓ 4↑	2↓ 3↑
CAP2	Adenylyl cyclase-associated protein	Interaction with actin	1↑	4↓			1↓	
CEP170B	Centrosomal protein of 170 kDa protein B	Microtubule organisation; centrosome		2↑			1↓	1↓

(Continues)

TABLE 3 (Continued)

			EC I–II	EC III–IV	EC V–VI	FC I–II	FC III–IV	FC V–VI
IQSEC1	IQ motif and SEC7 domain-containing protein 1	Endocytosis of plasma membrane proteins; E-cadherin recycling and actin cytoskeleton remodelling; enriched in the frontal cortex					1↑	1↓
GFAP	Glial fibrillary acidic protein	Cytoskeleton of astrocytes					2↓	
VIM	Vimentin	Major intermediate filament in mesenchymal cells					1↓	
FEZ1	Fasciculation and elongation protein Z − 1	Axon elongation in *C. elegans*				1↑	1↓	
MYH9	Myosin 9	Actin-binding protein		1↓	1↓			
MYL12A	Myosin regulatory like	Myosin heavy chain binding			2↑			
CTNNA1	Catenin alpha 1	Anchorage of actin filaments to the sarcolemma			1↑			
CTNNA2	Catenin alpha 2	Binding cadherins and actin-containing filaments of the cytoskeleton	1↑	1↑	2↑	1↓	4↑	1↑
CTNND2	Catenin delta	Connecting cadherins to actin filaments	2↓	1↓ 1↑	1↑			
ANK2	Ankyrin-2	Link the integral membrane proteins to the spectrin-actin cytoskeleton		2↓ 2↑	1↓	1↓	1↓ 1↑	
ANK3	Ankyrin-3	Clustering of voltage-gated sodium channels at the axon hillock	1↓ 1↑	1↑	4↓			
ANKRD13D	Ankyrin repeat domain-containing protein 13D	Ubiquitin-binding protein; negative regulation of receptor internalization		2↑				
VCL	Vinculin	Anchoring actin to membranes		1↓				
PALM	Paralemmin 1	Component of the cytoplasmic face of the plasma membranes	1↑	4↑	1↑			
SPTBN1	Spectrin beta chain, non-erythrocytic 1	Binding the plasma membrane to the cytoskeleton	1↓	1↓	1↓ 1↑	1↓	1↓ 1↑	
CAMSAP1	Calmodulin-regulated spectrin-associated protein 1	Stabilization of the microtubules			1↓			
CDH10	Cadherin	Cell adhesion molecule (CAM); calcium dependent transmembrane protein linked to cell junctions						1↓
ADD1	Adducin 1	Assembly spectrin-actin network	1↓		1↓	1↓ 1↑	1↓	
ADD2	Adducin 2			1↓ 1↑	1↓	2↓		1↑
ADD3	Adducin 3				1↓			
TJP1	Tight junction protein 1	Membrane-associate guanylate kinase (MAGUK) homologues; link F-actin to trans-membrane proteins; TJP1 enriched in the post-synaptic membrane		1↓	2↓	2↓		
TJP2	Tight junction protein ZO-2		1↑	1↑				

(Continues)

TABLE 3 (Continued)

			EC I–II	EC III–IV	EC V–VI	FC I–II	FC III–IV	FC V–VI
MPP2	Membrane palmitolated protein 2	Member of MAGUK proteins family, interaction with the cytoskeleton, regulation of intracellular junctions		2↑	2↑			
L1CAM	Neural cell adhesion molecule 1 (NCMA; CD56)	Cell-cell adhesion, synaptic plasticity		2↓			1↓	1↓
LSP1	Lymphocyte-specific protein	F-actin-binding protein in endothelia and blood cells		1↓			1↓	1↑
ARHGEF2	Rho-guanine nucleotide exchange factor 2	Activate GTPases; facilitate actin dynamics		1↑		1↓		
ARHGEF7	Rho-guanine nucleotide exchange factor 7			1↓				
ARHGAP35	Rho GTPase-activating protein 35	Activates G proteins and their GTPase activity				1↓		1↑
ARHGAP39	Rho GTPase-activating protein 39	Activates G proteins and their GTPase activity	1↑					
ARHGAP1	Rho-GTPase activating protein 1	Activates G proteins and their GTPase activity		1↓				
PKP4	Plakophilin-4	Cadherin-binding protein					1↑	2↓
MARCKS	Myristolated alanine-rich C-kinase substrate	Actin and calmodulin binding				1↓	1↑	1↑
MARCKSL1	MARCKS-related protein	When phosphorylated by MAPK8, induces actin bundles formation and stabilization, thereby reducing actin plasticity					1↓	
CPNE6	Colpine-6	Calcium-dependent membrane-binding protein					1↑	1↑
ANLN	Actin-binding protein anillin	Actin-binding protein					3↑	
ABLIM1	Actin-binding LIM protein	Actin-binding protein				1↑		
GMP6A	Neuronal membrane glycoprotein M6-a	Extracellular matrix assembly; organization actin cytoskeleton; GMP6A expressed in neurons, GMP6B expressed in neurons and glial cells				1↓	1↑	
GMP6B	Neuronal membrane glycoprotein M6-b					1↓		
PNN	Pinin	Cell adhesion; RNA splicing				1↑	1↓	
SYNPO2	Synaptopodin	Actin-binding protein, transport				1↑		2↓
PVRL1 nectin1	Nectin cell adhesion molecule 1	Calcium-independent cellular adhesion		1↓	1↓			
GAP43	Growth associated protein 43	Protein associated with axonal cone growth		1↓	1↓		1↓	1↓
CRMP1	Collapsin response mediator protein 1	The encoded protein is thought to be a part of the semaphorin signal transduction pathway implicated in semaphorin-induced growth cone collapse during neural development		2↑	1↓	1↓	1↑	

(Continues)

TABLE 3 (Continued)

			EC I–II	EC III–IV	EC V–VI	FC I–II	FC III–IV	FC V–VI
MAG12	Membrane associated guanylate kinase	MAGUK protein; localized at the junctional complexes and synapses	1↑					
CCDC6	Coiled-coil domain-containing protein 6	Protein of the cytoskeleton		1↑				
TMEM233	Transmembrane protein 233	Interferon-induced transmembrane domain-containing protein D2; multi-pass membrane domain	1↑		1↑			
LMNA	Prelamin-A7C	Stability of the nuclear membrane	1↑		1↑	1↓	1↓	
EPB41L1	Band 4.1-like protein 1	Stabilizes D2 and D3 receptors at the plasma membrane	1↑	1↓ 3↑	2↑	2↓	1↓ 1↑	2↑
EPB41L2	Band 4.1-like protein 2	Required for dynein-dynactin complex	1↓			1↑		1↓
EPB41L3	Band 4.1-like protein 3	Cytoskeletal anchoring at the plasma membrane		1↓ 1↑	1↓	1↑		X
DMD	Dystrophin	Anchors the extracellular matrix to the cytoskeleton via F-actin				1↑		
ABI2	Abl interactor 2	Regulator of actin cytoskeleton dynamics underlying cell motility and adhesion		1↓ 1↑	1↓			
CCDC92	Coiled-coil domain-containing protein 92	Localized in the cytoskeleton and cytoplasm; unknown function					1↓	1↓
SGIP1	SH3GL interacting endocytic adaptor 1	Localization: cytoskeleton; signaling by receptors in neuronal systems involved in energy homeostasis via its interaction with endophilin		3↑	1↑	1↑	1↓	3↓
DMTN	Dematin	Membrane-cytoskeleton-associated protein with F-actin-binding activity that induces F-actin bundles formation and stabilization		1↑			1↓	
TAGLN2	Transgelin	Actin filament binding			1↑			
SHROOM2	Protein shroom2	Cell junctions					1↓	
MLLT4	Afadin	Zonula adherens					1↓	
DST	Dystonin	Integrator of intermediate filaments	1↓					
MAP4	Microtubule associated protein 4	Microtubule binding			1↓			
SORBS1	Sorbin and SH3 domain-containing protein	Intermediate filaments; target of myb1 like 2 membrane trafficking protein				1↑		
KBTBD11	Kelch repeat and BTB domain-containing protein 11	Localized in plasma membrane, iunteraction with Intermediate filaments				1↑		
C14orf37/ ARMH4	Armadillo like helical domain containing 4	Integral component of the membrane						2↓

(Continues)

TABLE 3 (Continued)

			EC I–II	EC III–IV	EC V–VI	FC I–II	FC III–IV	FC V–VI
ITSN1	Intersectin-1	Interacts with golgin to couple the Golgi apparatus with the actin network	1↑					
GPM6B	Neuronal membrane glycoprotein M6B	Component of rafts				1↓		
SYNM	Synemin	Component of the cytoskeleton			1↑			
Synapsis and dense core vesicles								
SYN1	Synapsin-1	Bundles actin and enhances spectrin binding; enriched in pre-synaptic terminals		3↑				
SYN3	Synapsin-3	Cytoplasmic surface of the synaptic vesicle		1↑				
STXBP1	Syntaxin-binding protein	Regulation of the transmembrane attachment protein receptor syntaxin; neurotransmitter release	1↑	2↑				
RIMS1	Regulating synaptic membrane exocytosis 1	Regulation of synaptic vesicle exocytosis and neurotransmitter release		1↓				
RPH3A	Rabphilin 3A	In the pre-synaptic terminal modulates Rab3a-dependent synaptic vesicle trafficking and calcium-triggered neurotransmitter release; in the post-synaptic compartment, regulates NMDA receptor stability		1↓		1↑		
BSN	Protein Basson	Organization of the pre-synaptic cytoskeleton	1↓	3↑	1↓ 1↑		1↓	1↑
SV2A	Synaptic vesicle glycoprotein 2A	Prototypic synaptic membrane protein regulating action potential-dependent neurotransmitters release			3↑			
SV2B	Synaptic vesicle glycoprotein 2B	Synaptic membrane protein regulating action potential-dependent neurotransmitters release				1↓		
PCLO	Protein Piccolo	Component of the pre-synaptic cytoskeleton				1↓ 2↑	1↑	
CHGA	Chromogranin A	Member of the granin family of neurosecretory proteins; modulation of neuroendocrine function			1↑			
GRM5	Metabotropic glutamate receptor 5	Glutamatergic neurotransmission		2↑		1↓	2↑	2↑
DLGAP1	Disks large-associated protein 1	Binds to PSD-95 and facilitates the assembly of the post-synaptic density of neurons	1↓	1↓			1↑	1↓
SYP	Synaptophysin	Synaptic vesicle glycoprotein						1↑
PPHLN1	Periphilin-1	Found in the soluble fraction of bovine chromaffin secretory vesicles (function not known in brain)				1↑	1↓	1↓

(Continues)

TABLE 3 (Continued)

			EC I–II	EC III–IV	EC V–VI	FC I–II	FC III–IV	FC V–VI
ANKS1B	Ankyrin repeat and sterile alpha motif domain-containing protein 1B	Regulation of synaptic plasticity by receptor localization to synapse					1↑	
SHANK	SH3 and multiple ankyrin repeat domain protein	Major scaffold postsynaptic density protein which interacts with multiple proteins and complexes to orchestrate the dendritic spine and synapse formation		1↑				
DLG2	Disks large homolog 2	Stabilization of synapses						1↓
PSD	PH and Sc7 domain-containing protein	Post-synaptic		1↑	1↓			
DBN1	Debrin	Postsynaptic, cytosol				1↑		
SPARCL1	Sparc-like protein 1	Calcium binding; synaptic membrane adhesion			1↓			
Myelin								
MBP	Myelin basic protein	Myelin protein	3↓	2↓	2↓			
PLP1	Myelin proteolipid protein	Major myelin protein of the CNS		1↓	1↓			
CNP	2′,3′-cyclic nucleotide 3′ phosphodiesterase	4% of total myelin proteins; also binds to microtubules	1↓		1↓			
ADAM22	ADAM metallopeptidase domain 22	Integrin ligand, involved in myelination; lacks metaloprotease activity		1↓				
Membrane transport and ion channels								
ATP1A1	Sodium/potassium transporting ATPase subunit alpha-1	Catalyze the hydrolysis of ATP coupled with exchange of sodium and potassium ions across the plasma membrane		1↓	1↓	1↓	1↓ 1↑	1↓
ATP1A2	Sodium/potassium transporting ATPase subunit alpha-2			1↓	1↓			1↓
ATP1A3	Sodium/potassium transporting ATPase subunit alpha-3			1↓	1↓			1↓
ABCA2	ATP binding cassette subfamily B member 2	Transport across intra- and extracellular membranes	1↓		2↓			
ATP8A1	Phospholipid transportin ATPase IA	ATPase-coupled cation transmembrane transporter			1↑	2↓		3↑
SLC6A17	Sodium-dependent neutral amino acid transporter SLC6A17	Amino acid transport; localizes at synaptic junctions particularly in excitatory glutamatergic terminals			1↑			
RTN1	Reticulon 1	Involved in neuroendocrine secretion or in membrane trafficking in neuroendocrine cells					1↓	
RTN3	Reticulon 3	Modulate the activity of beta-amyloid converting enzyme 1 (BACE-1), and the production of β-amyloid	1↑	1↑		1↑	2↑	

(Continues)

TABLE 3 (Continued)

			EC I–II	EC III–IV	EC V–VI	FC I–II	FC III–IV	FC V–VI
RTN4	Reticulon 4	Localization in the endoplasmic reticulum (ER); morphogenesis of the endoplasmic reticulum; proper localization of proteins in the ER; interaction with BACE1	1↓		1↓ 1↑	1↓	1↑	1↑
CRMP1	Collapsin response mediator protein	Semaphoring signal transduction pathway; regulator of growth cone collapse		2↑				
PRRT2	Proline-rich transmembrane protein	Membrane transport					1↓ 2↑	1↑
GNAO1	Guanine nucleotide-binding protein G(o) subunit α	Modulators in various transmembrane signaling systems				1↑	1↓	1↓
STMN2	Stathmin2	Cytoplasmic transport of vesicles; regulator of microtubule stability. When phosphorylated by MAPK8, stabilizes microtubules and consequently controls neurite length in cortical neurons				1↑	1↓	1↓
GNG10	Guanine nucleotide-binding protin G(I)/G(S)/G(0) subunit gamma	G protein coupled receptor signalling pathway; cellular response to catecholamine stimulus					1↓	
STMN1	Stathmin1	Regulation of the microtubule filament system by destabilizing microtubules. It prevents assembly and promotes disassembly of microtubules				1↑		1↓
ASAP1	ArfGAP with SH3 domain, ankyrin repeat and PH domain 1	Membrane trafficking				1↑	1↓	1↓
HCN2	Potassium/sodium hyperpolarization-activated cyclic nucleotide-gated ion channel 2	Channel of unknown function in brain					1↑	1↑
CACNG3	Voltage-dependent calcium channel gamma 3 subunit	Regulates the trafficking to the somatodendritic compartment and gating properties of AMPA-selective glutamate receptors. Promotes their targeting to the cell membrane and synapses and modulates their gating properties		1↑				

(Continues)

TABLE 3 (Continued)

			EC I–II	EC III–IV	EC V–VI	FC I–II	FC III–IV	FC V–VI
KCNAB2	Voltage-gated potassium channel subunit beta-2	Localization plasma membrane and cytoskeleton; regulation of potassium ion transmembrane transport		1↑				
SCN2A	Sodium channel protein type 2 subunit alpha	Mediates the voltage-dependent sodium ion permeability of excitable membranes		1↓	1↓	1↑		1↓
PITPNM3	Membrane associated phosphatidylinosoitol transfer protein 3	Transport of phospholipids to the cell membranes	1↑					
SPTBN2	Spectrin beta chain, non-erythrocytic 2	Regulates glutamate transporter pathway at the cell membrane				1↓		1↑
SLC9A1	Solute carrier family 9 member A1	Sodium/hydrogen exchanger; plasma membrane transporter					1↑	
SLC4A4	Solute carrier family 4 member 4	Electrogenic sodium bicarbonate cotransporter 1 in the membrane		1↑				
SLC14A1	Solute carrier family 14	Urea and water transmembrane transport					1↓	
CADPS	Calcium-dependent secretion activator	Peripheral membrane protein required for Ca2+-regulated exocytosis of secretory vesicle				1↓		
HEPACAM	Hepatic and glial cell adhesion molecule	Protein localized to the cytoplasmic side of the plasma membrane, involved in cytoplasm-matrix interactions					1↓ 1↑	
SEC31A	SEC31 homolog A, COPII coat complex component	Component of the outer layer of the coat protein complex II	1↓				1↓	

Note: Dysregulated phosphoproteins are marked with as many ↓ or ↑ as the number of phosphosyte sites, indicating hyper- or hypophosphorylation. Note that several proteins may have two or more phosphorylation sites with opposite directions.

dysregulated phosphoproteins occurred at stages III–IV in the EC and FC. This finding suggests that the greatest phosphorylation-related activity (hyper- and hypophosphorylation) occurs at the middle stages of NFT pathology.

To learn about the possible implications of dysregulated phosphoproteins linked to the structure and function of cell membranes, synapses, cytoskeleton, and the pathway of β-amyloid formation, β-amyloid precursor protein (APP), presenilin1 (PSEN1), presenilin 2 (PSEN2), β-secretase 1 (BACE1), BACE 2 and apolipoprotein E (ApoE4), together with the components of the γ-secretase complex aph-1 homolog A, γ-secretase subunit (APH1A), APH1B, nicastrin (NCT/NCSTN), and presenilin enhancer γ-secretase subunit (PEN2/PSENEN), and the modulators neprilysin (NEP/MME) and insulin-degrading enzyme (IDE) (44), were all incorporated into the interactome (Figure 5). In addition to several direct and indirect interactions, close interaction among the components of the β-amyloid pathway and two membrane proteins located in the membrane of the endoplasmic reticulum, RETN3, and RETN4, was noted in the different stages and regions (Figure 5).

3.6 | Molecular synaptic derangements in the EC and FC across NFT stages

We wanted to evaluate the existence of molecular similarities and differences at the synaptic level in the EC and FC across NFT staging. To do this, the SynGO tool was used (45) to categorize synaptic locations and synaptic processes derived from our anatomo-proteomic datasets. Several proteins linked to synapse were abnormally regulated. In the EC, stages I–II: 37; stages III–IV: 67, and stages V–VI: 56. In the FC, stages I–II: 34, stages III–IV: 32, and stages V–VI: 32. These were analyzed separately using SynGO according to biological process (BP) and cellular component

TABLE 4 Dysregulated phosphorylation of kinases, proteins linked to DNA or protein deacetylation, proteins linked to gene transcription and protein synthesis, heat-shock proteins, members of the ubiquitin-proteasome system (UPS), and proteins involved in energy metabolism in the entorhinal cortex (EC) and frontal cortex area 8 (FC) at different stages of NFT pathology (stages I–II, III–IV and V–VI of Braak) compared with middle-aged individuals

			EC I–II	EC III–IV	EC V–VI	FC I–II	FC III–IV	FC V–VI
Kinases								
DCLK1	Serine/theronine protein kinase DCLK1	Integral component of plasma membrane and post-synaptic density; protein kinase activity		1↓				
PRKAR2B	cAMP-dependent protein kinase type II-beta regulatory subunit	Colocalizes with PJA2 (Praja Ring Finger Ubiquitin Ligase 2) in the cytoplasm and at the cell membrane; activation of PKA and regulation of GDK3 activity; mediates membrane association by binding to anchoring proteins, including the MAP2 kinase	1↑	1↓ 1↑				
BRSK1	Serine/threonine protein kinase BRSK1	Localization in the cytoskeleton, and synapses; phosphorylates CDC25B, CDC25C, MAPT/TAU, RIMS1, TUBG1, TUBG2 and WEE1		1↑	1↑			
BRSK2	Serine/theronine protein kinase BRSK2	Localization in the cytoskeleton, endoplasmic reticulum and perinuclear region; phosphorylates CDK16, CDC25C, MAPT/TAU, PAK1 and WEE1		1↑				
PACSIN1	Protein kinase C and casein kinase substrate in neurons protein 1	Decreases microtubule stability and inhibits MAPT-induced microtubule polymerization; participates in cellular transport processes by recruiting DNM1, DNM2 and DNM3 to membranes; plays a role in the reorganization of the actin cytoskeleton		1↓				1↓
SRCIN1	SRC kinase signalling inhibitor 1	Negative regulator of non-receptor protein tyrosine kinase; regulates dendritic spine morphology; involved in calcium-dependent exocytosis; plays a role in neurotransmitter release or synapse maintenance		1↑			1↑	
GSK3A	Glycogen synthase kinase 3 alpha	Constitutively active protein kinase that acts as a negative regulator in the hormonal control of glucose homeostasis, Wnt signaling and regulation of transcription factors and microtubules		1↓				
CAMK2A	Calcium-calmodulin-dependent protein kinase type II subunit alpha	Localization cytoplasm, synapses; involved in synaptic plasticity, neurotransmitter release and long-term potentiation; phosphorylation of Thr-286 locks the kinase into an activated state		1↓	1↓			1↓
CAMK2B	Calcium-calmodulin-dependent protein kinase type II subunit beta	Reorganization of the actin cytoskeleton during plasticity by binding and bundling actin filaments in a kinase-independent manner; autophosphorylation of Thr-287 which turns the kinase in a constitutively active form after activation by Ca^{2+}/calmodulin	1↓	2↓	2↓	1↓	2↑	

(Continues)

TABLE 4 (Continued)

			EC I–II	EC III–IV	EC V–VI	FC I–II	FC III–IV	FC V–VI
PAK1	Serine/threonine protein kinase PAK1	Role in cytoskeleton dynamics, in cell adhesion, migration, proliferation, apoptosis, mitosis, and in vesicle-mediated transport processes Phosphorylates and activates MAP2K1, and thereby mediates activation of downstream MAP kinases		1↑	X	1↑		
AKAP-12	A-kinase anchoring protein 12	Regulatory subunit of protein kinase A (PKA); PKA phosphorylates and deactivates proteins that have the motif Arginine-Arginine-X-Serine exposed; involved in multiple cellular signaling pathways; AKAP-12 anchors PKA at the cplasma membrane and mitochondria	1↑	1↑	2↑			
AAK1	AP2 associated kinase 1	The protein interacts with and phosphorylates a subunit of the AP-2 complex, which promotes binding of AP-2 to sorting signals found in membrane-bound receptors and subsequent receptor endocytosis		1↑	1↑	1↓		1↓
CAMK4	Calcium-calmodulin-dependent protein kinase type IV	Regulates the activity of several transcription activators, such as CREB1, MEF2D, JUN and RORA; can activate the MAP kinases MAPK1/ERK2, MAPK8/JNK1 and MAPK14/p38 and stimulate transcription through the phosphorylation of ELK1 and ATF2; mainly involved in intracellular signal transduction			1↓			
MAST1	Microtubule-associated serine/threonine-protein kinase	Links the dystrophin/utrophin network with microtubule filaments via the syntrophins; cyoskeletal organization; intracellular signal transduction	1↓		1↓			
PRKCG	Protein kinase C gamma type	Regulation of the neuronal receptors GRIA4/GLUR4 and GRIN1/NMDAR1; modulation of receptors and neuronal functions related to sensitivity to opiates, pain and alcohol; mediation of synaptic function; chemical synaptic transmission; intracellular signal transduction			1↓	1↓	1↓	1↓
PRKCE	Protein kinase C epsilon type	Regulation of multiple cellular processes linked to cytoskeletal proteins, such as cell adhesion, motility, migration and cell cycle, functions in neuron growth and ion channel regulation; phosphorylates MARCKS	1↑		1↑			
PRKAB2	5′-AMP-activated protein kinase subunit beta-2	Non-catalytic subunit of AMP-activated protein kinase (AMPK). In response to reduction of intracellular ATP levels, AMPK activates energy-producing pathways and inhibits energy-consuming processes: inhibits protein, carbohydrate and lipid biosynthesis			1↑			

(Continues)

TABLE 4 (Continued)

			EC I–II	EC III–IV	EC V–VI	FC I–II	FC III–IV	FC V–VI
PRKRA	Interferon-inducible double-stranded RNA-dependent protein kinase activator Ai	Activates EIF2AK2/PKR in the absence of double-stranded RNA (dsRNA), leading to phosphorylation of EIF2S1/EFI2-alpha and inhibition of translation and induction of apoptosis. Required for siRNA production by DICER1 and for subsequent siRNA-mediated post-transcriptional gene silencing	1↑		1↑			
WNK1	Serine/threonine-protein kinase WKN1	Dynamic behavior of the intermediate filament cytoskeleton by phosphorylation of vimentin; localized in the perinuclear region					1↓	1↓
CAMK2D	Calcium-calmodulin-dependent protein kinase type II subunit delta	ATP binding, calmodulin binding, calmodulin-dependent protein kinase activity, ion channel binding, protein homodimerization activity, titin binding, protein serine/threonine kinase activity, sodium channel inhibitor activity, titin binding; main function in heart and skeletal muscle				1↓		
STK32C	Serine/threonine protein kinase 32C	Intracellular signal transduction				1↓		
NUAK1	NUAK family SNF1-like kinase 1	Intracellular signal transduction; protein phosphorylation; regulation of senescence					1↑	
MINK1	Misshapen kinase 2	Negative regulator of Ras-related Rap2-mediated signal transduction to control neuronal structure and AMPA receptor trafficking	1↓					
MAGI2	Membrane-associated guanyl kinase, WW and PDZ domain	Alpha-actinin binding; cell surface receptor signalling pathway	1↑					
Proteins linked to DNA or protein deacetylation								
TERF2IP	Telomeric repeat-binding factor 2-interacting protein	Acts both as a regulator of telomere function and as transcription regulator		1↑	1↑			
HDAC2	Histone deacetylase 2	Deacetylation of lysine residues on the N-terminal part of the core histones (H2A, H2B, H3 and H4); histone deacetylation gives a tag for epigenetic repression			1↓			
SUDS3	Sin3 histone deacetylase corepresor complex component SD53	Regulatory protein which represses transcription and augments histone deacetylase activity of HDAC1			1↑			
SIRT2	NAD-dependent protein deacetylase sirtuin 2	NAD-dependent protein deacetylase, which deacetylates internal lysines on histone and alpha-tubulin as well as many other proteins such as key transcription factors			2↓			
FGF12	Fibroblast growth factor 12	Growth factor; lacks N-terminal sequence of most FGF member; nuclear localization		1↓	1↓			
TP53BP1	Tumor suppressor 53-binding protein 1	DNA repair				1↑		1↓

(Continues)

TABLE 4 (Continued)

			EC I–II	EC III–IV	EC V–VI	FC I–II	FC III–IV	FC V–VI
Proteins linked to gene transcription and protein synthesis								
RPLP1	60S acidic ribosomal protein P1	Structural component of the large ribosomal subunit		1↓	1↓	2↓		
RPLP0	60S acidic ribosomal protein P0	Component of the large ribosomal subunit rRNA binding		1↓			2↓ 1↑	
CTIF	CBP80/20-dependent translation initiation factor	mRNA translation mediated by the cap-binding complex, that takes place during or right after mRNA export via the nuclear pore complex		4↓	1↓		1↓	1↓
RNPS1	RNA binding protein with serine rich domain 1	Nucleocytoplasmic shuttling protein of mRNAs	2↑	2↑	2↑			
PML	PML nuclear body scaffold	Member of the Trim family. localizes to nuclear bodies where it functions as a transcription factor		1↑	1↑			
C6orf203: MTRES1	mitochondrial transcription rescue factor 1	C6orf203 is an RNA-binding protein involved in mitochondrial protein synthesis		2↓	1↓			
EIF3J	Eukaryotic translation initiation factor 3J	EIF3J is one of thirteen subunits of eukaryotic translation initiation factor 3, the largest complex of the translation initiation factors						1↓
EIF5	Eukaryotic translation initiation factor 5	Catalyzes the hydrolysis of GTP bound to the 40S ribosomal initiation complex with the subsequent joining of a 60S ribosomal subunit			2↑			1↑
EIF4B	Eukaryotic translation initiation factor 4 beta	eIF4B phosphorylation at Ser504 links synaptic activity with protein translation		1↓	1↓ 1↑			
EEF1B2	Elongation factor 1 beta	Guanyl-nucleotide exchange activity; translation elongation factor activity						1↓
SRRM1	Serine/arginine repetitive matrix protein 1	RNA splicing factor	1↑	2↓	2↓			
SRRM2	Serine/arginine repetitive matrix protein 2	RNA splicing factor	1↓	4↓	3↓	2↑	2↓	
SRSF6	Serine/arginine-rich splicing factor 6	Plays a role in the alternative splicing of MAPT/Tau exon 10		1↓				
SRSF10	Serine/arginine-rich splicing factor 10	In its dephosphorylated form acts as a general repressor of pre-mRNA splicing						1↑
MATR3	Matrin-3	Internal nuclear framework				1↑	1↓	1↓
SMARCA5	SWI/SNF-related matrix associated actin dependent regulator of chromatin subfamily A member 5	Regulator of gene transcription modulating chromatin around selected genes				1↑	1↓	1↓
GATAD2B	Transcriptional repressor p66-beta	Transcriptional repressor				2↑		
MFAP1	Microfibrillar associated protein 1	Component of the spliceosome B complex				2↓		2↑
SLU7	Pre-mRNA-splicing factor SLU7	Component of the spliceosome					1↓	
HNRNPUL2	Heterogeneous nuclear ribonucleoprotein U-like protein 2	RNA binding; localization in the nucleus					1↓	

(Continues)

TABLE 4 (Continued)

			EC I–II	EC III–IV	EC V–VI	FC I–II	FC III–IV	FC V–VI
YAP1	Transcriptional coactivator YAP1	Transcription regulator	1↑		2↑			
GNL1	G protein nucleolar 1	GTPase essential for ribosomal pre-rRNA processing and cell proliferation		1↑				
NUCKS1	Nuclear ubiquitous casein and cyclin dependent kinase substrate 1	DNA-binding transcription activator activity, RNA polymerase II-specific		2↓	1↓			2↑
PURB	Transcriptional activator protein Pur-beta	Binds repeated elements in single-stranded DNA					1↑	
BCLAF1	BCl-2 associated transcription factor	DNA and RNA binding; regulator of apoptosis				1↓		
ATRX	Transcriptional regulator ATRX	Chromatin remodeling		1↓				
POLE4	DNA polymerase epsilon subunit 4	DNA replication initiation; telomere maintenance					1↓	
HRNPH2	Heterogeneous nucler ribonucleoprotein H2	Regulation of RNA splicing	1↑					
HRNPC	Heterogeneous nuclear ribonucleoproteins C1/C2	Binds pre-mRNA and nucleates the assembly of 40S hnRNP particles	1↑					
ACIN1	Apoptotic chromatin condensation inducer in the nucleus	Nucleic acids binding					2↓	
Heat-shock proteins								
HSP90AB1	Heat-shock protein HSP-90-beta	Assist the conformational folding or unfolding and the assembly or disassembly of proteins		2↓	2↓			
HSPA12A	Heat-shock protein 70 kDa 12A			1↑	1↑			
DNAJA4	DnaJ heat-shock protein family (Hsp40) member A4			1↓	1↓			
HSPB1	Heat-shock protein beta-1				1↑			
CDC37	Hsp90 co-chaperone Cdc37				1↓			
HSPA4L	Heat-shock protein 70 kDa protein 4L					1↑		
HSP90AA1	Heat-shock protein HSP 90alpha				1↓			
Members of the ubiquitin proteasome system								
UCHL1	Ubiquitin-carboxyl-terminal hydrolase isozyme 1	Ubiquitin-protein hydrolase involved both in the processing of ubiquitin precursors and of ubiquitinated proteins		1↓				
UBR4	E3 ubiquitin protein ligase UBR4	Recognizes and binds to proteins bearing specific N-terminal residues for their subsequent degradation		1↓				
USP24	Ubiquitin carboxyl-terminal hydrolase 24	Thiol-dependent ubiquitin-specific protease activity		1↓				
UB2O	E2/E3 hybrid ubiquitin-protein ligase UBE20	E2/E3 hybrid ubiquitin-protein ligase that displays both E2 and E3 ligase activities and mediates monoubiquitination of target proteins		1↑				

(Continues)

TABLE 4 (Continued)

			EC I–II	EC III–IV	EC V–VI	FC I–II	FC III–IV	FC V–VI
TRIM2	Tripartite motif containing 2	Ubiquitin-conjugating enzyme E2 D1-dependent E3 ubiquitin-protein ligase	2↓	2↓ 1↑	3↓ 1↑			
PSMA5	Proteasome subunit alpha type-5	Component of the proteasome, a multicatalytic proteinase complex				1↑		
UFD1L	Ubiquitin fusion degradationprotein 1 homolog	Polyubiquitin modification-dependent protein binding						1↑
Energy metabolism								
TALDO1	transaldolase	Pentose phosphate pathway	1↓	1↓ 1↑	1↓			
PGM2L1	Glucose 1,6-bisphosphate synthase	Catalyzes the transfer of a phosphate to glucose-1-phosphate yielding to glucose-1–6-bisphosphate		1↓	1↓			
GAPDH	Glyceraldehyde 3 phosphate dehydrogenase	Catalyzes the sixth step of glycolysis				2↑		1↓
ATP5B	ATP synthase 1 beta mitochondrial	Mitochondrial membrane ATP synthase (complex V), production of ATP			1↓			1↓
PGM1	Phosphoglucomutase-1	Phosphohexose mutase			1↓	1↑	1↓	
PGM3	Phosphoacetylglucosamine mutase	Involved in step 2 of the subpathway that synthesizes N-acetyl-alpha-D-glucosamine 1-phosphate from alpha-D-glucosamine 6-phosphate			1↓			
MDH1	Malate dehydrogenase	Mitochondrial enzyme, oxidation of malate to oxaloacetate, participation in the citric acid cycle			1↑			
MTFR1L	Mitochondrial fission regulator 1-like	Regulate mitochondrial organization and fission			1↑			
MDAH1	Malate dehydrogenase cytoplasmic	Assisting the malate-aspartate shuttle from the cytoplasm to the mitochondria			1↑			
PGK1	Phosphoglycerate kinase 1	First ATP-generating step of the glycolytic pathway				1↑	1↓	1↓
BCKDHA	2-oxoisovalerate dehydrogenase subunit alpha, mitochondrial	Conversion of alpha-keto acids to acyl-CoA and CO_2; localization mitochondrial matrix				1↑	1↓	1↓
ALDOC	Fructose-bisphosphate aldolase C	Involved in the step 4 of the pathway that synthesizes D-glyceraldehyde 3-phosphate and glycerone phosphate from D-glucose						2↑
PKM	Piruvate kinase	Last step of glycolysis; transfer of a phosphate group from phosphoenolpyruvate to adenosine diphosphate yielding one molecule of pyruvate and one ATP					1↓	
TPI1	Triosephosphate isomerase	Glycolytic enzyme that catalyses the reversible interconversion of glyceraldehyde 3-phosphate and dihydroxyacetone phosphate	1↑					1↓

Note: Dysregulated phosphoproteins are marked with as many ↓ or ↑ as the number of phosphosyte sites, indicating hyper- or hypophosphorylation. Note that several proteins may have two or more phosphorylation sites with opposite directions.

(CC). Lists may be seen in Table S6. Synaptic interactomes showed that the synaptic homeostasis was disrupted the most in the EC at the III–IV stage (Figure 6). Several direct and indirect interactions among the components of the β-amyloid pathway and altered synaptic proteins were noted in the different stages and regions when components of the β-amyloid pathways were incorporated into the interactome (Figure 6).

3.7 | Immunohistochemistry and double-labeling immunofluorescence and confocal microscopy

A few antibodies directed against the identified proteins in the present study were commercially available. Some of them do not work for immunohistochemistry. A selection of antibodies was utilized to validate phosphoproteomics. Also, we used other phospho-specific antibodies based on the hypothesis that some phosphoproteins were not detected in our phosphoproteomics approach due to instrument sensitivity and TiO2 phosphopeptide enrichment-based selectivity. Antibodies against ADD1-P, ADD1/ADD2-P, MAP2-P, and PAK1-P were chosen for validation of cytoskeletal components; antibodies against NFL-P, kinases p38-P and SAPK/JNK-P, and non-phospho-specific antibodies against NFM and NFH were added for study. The selection of the late proteins was based on the fact that the expression of p38-P and SAPK/JNK-P was already described in advanced stages of sAD (46-48), and increased expression of neurofilaments was already detected in NFTs (49, 50). An antibody against catenin β-P was chosen because other members of the catenin family showed altered phosphorylation, but antibodies against those phosphorylated forms did not work in our hands.

In the EC, catenin β-P and p38-P immunoreactivity appeared at the first and middle stages of NFT pathology as small granules in the cytoplasm of a subpopulation of neurons. This pattern was also found for p38-P in many neurons of the EC at stages V–VI of NFT pathology. MA cases were not stained with MAP2-P and SAPK/JNK-P antibodies. NFTs were stained with MAP2-P and SAPK/JNK-P from the first stages of NFT pathology onwards; positive cells increased in number with stage progression. In MA and cases with NFT pathology, only rare filaments were stained with anti-NFL-P antibodies. Besides basal staining, a few NFTs were decorated with NFL-P antibodies. Similar staining was found with antibodies directed against non-phosphorylated NFM and NFH; a subpopulation of NFTs showed increased NFM and NFH immunoreactivity. In MA and cases with NFT pathology, the nucleus of neurons was dyed with anti-PAK1-P antibodies. PAK1-P immunoreactivity was marked in NFTs at stages III–IV and V–VI, but only as irregular or granular deposits in a few neurons at stages I–II. ADD1-P immunoreactivity was found in the cytoplasm of neurons and astrocytes in MA and cases with NFT pathology. Increased ADD1-P immunoreactivity occurred in astrocytes and a subpopulation of NFTs at middle and advanced stages of NFT pathology. A similar pattern was observed with anti-ADD1/ADD2-P antibodies. Images of selected immunostained sections in the EC are shown in Figure 7.

Regarding the FC, catenin β-P and p38-P immunoreactivity was found as small granules in the cytoplasm of very few neurons at the first and middle stages of NFT pathology. Catenin β-P also decorated a few NFTs, and p38-P was found in medium-size neuronal inclusions in a subpopulation of neurons at stages V–VI. A few cortical neurons showed MAP2-P and SAPK-JNK-P-immunoreactive cytoplasmic deposits, a few of them reminiscent of pre-tangles, at stages I–II and III–IV. NFTs were stained with MAP2-P and SAPK/JNK-P antibodies at stages V–VI. ADD1-P and ADD1/ADD2-P immunoreactivity was increased in the cytoplasm and processes of astrocytes, and in the cytoplasm of a subpopulation of neurons at middle and advanced stages of the disease. As occurred in the EC, a subpopulation of NFTs showed increased NFL-P, NFM, and NFH immunoreactivity in the cerebral cortex. Images of selected immunostained sections in the FC are shown in Figure 8, upper panel.

To elucidate the relationship if any between p38-P and catenin β-P-immunoreactive cytoplasmic granules and phospho-tau deposition in neurons, double-labeling immunofluorescence with p38-P or catenin β-P, and AT8 antibodies was examined with confocal microscopy. Double-labeling immunofluorescence and confocal microscopy of p38-P and AT8 in the FC at stages III–IV showed p38-P in small granules in neurons with early phospho-tau deposits. Double-labeling immunofluorescence and confocal microscopy of PAK1-P and AT8 in the EC at stages I–II disclosed PAK1-P-immunoreactive small granules in the cytoplasm of neurons at different stages of phospho-tau deposition, including pre-tangles and tangles (Figure 8, lower panel).

4 | DISCUSSION

Analysis of molecular profiles in the human brain has several limitations, mainly related to concomitant pathologies and post-mortem delay interval between death and tissue processing, as well as the region examined and stage of the disease; this is further complicated by the number of cases analyzed and the robustness of the methods employed (31, 51). The present study minimizes these limitations. In this line, it is important to stress the lack of comorbidities and concomitant pathologies in the present series (15). We analyzed the (phospho)proteomic profiles of two cortical regions, the EC and the FC. The MA control group must be not considered an age-matched control group but rather a baseline control of the scenario occurring in middle-aged individuals with no NFT pathology. It can be argued that phosphorylation changes observed at stages I–II in the present series may be related to aging. We have considered the hypothesis of AD as a continuum of an age-related biological process leading to degeneration that embodies NFT pathology, and this will be discussed below.

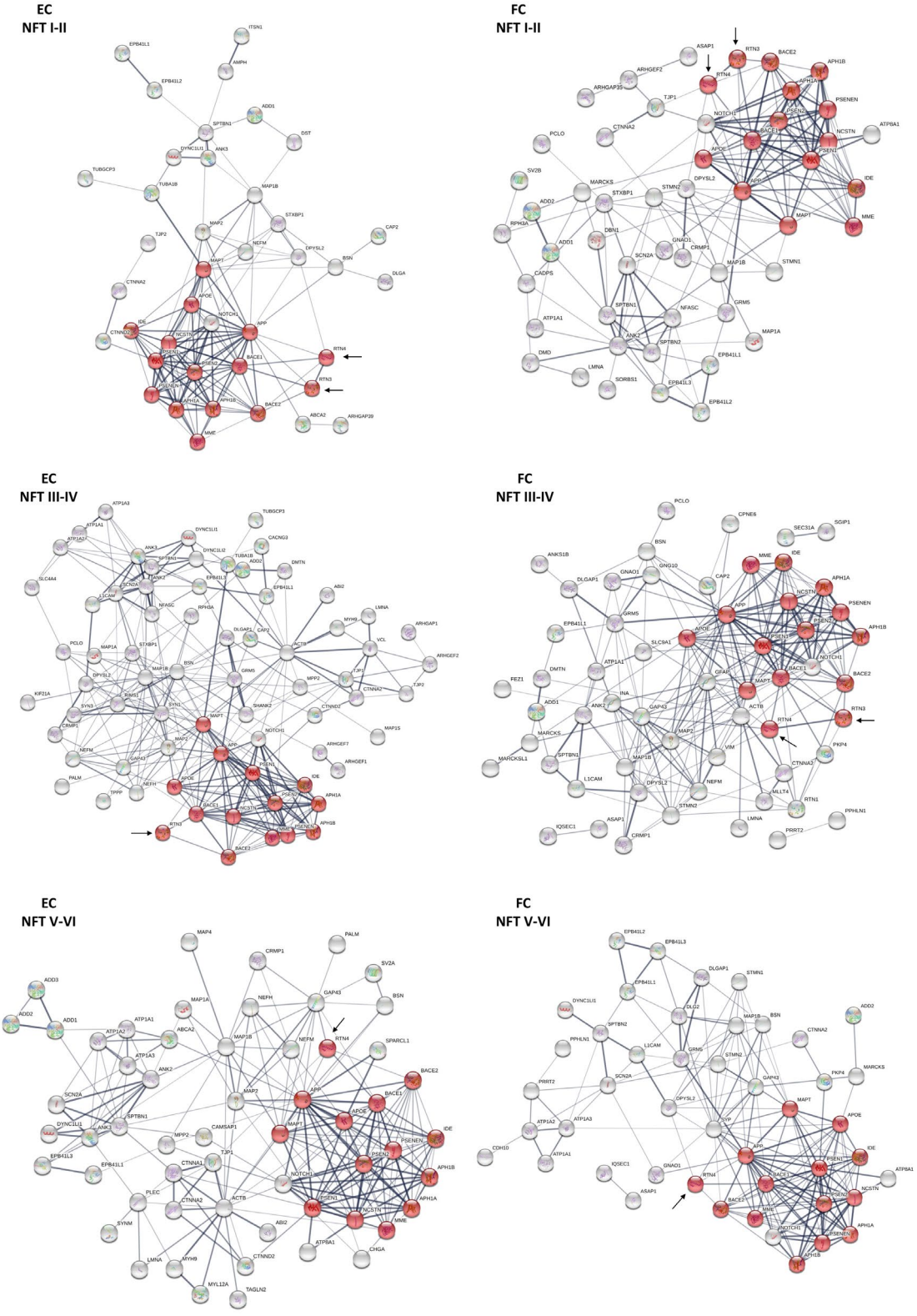

FIGURE 5 Interactomes of the dysregulated cytoskeletal, membrane, and synaptic (phospho)proteins in the entorhinal cortex (EC) and frontal cortex area 8 (FC) at different stages of NFT pathology (stages I–II, III–IV, and V–VI of Braak). A large number of (phospho)proteins are dysregulated at the first stages (I–II) in the EC and FC. Most dysregulation occurs at the middle stages (III–IV) of AD-related pathology. Dysregulated proteins were artificially combined with proteins linked to β-amyloid formation (red balls), including β-amyloid precursor protein (APP), presenilin1 (PSEN1), presenilin 2 (PSEN2), β-secretase 1 (BACE1), BACE 2, apolipoprotein E (ApoE4), aph-1 homolog A γ-secretase subunit (APH1A), APH1B, nicastrin (NCT/NCSTN), presenilin enhancer γ-secretase subunit (PEN2/PSENEN), neprilysin (NEP/MME), and insulin-degrading enzyme (IDE). Close interactions between the proteins of the membranes and cytoskeleton, and proteins of the β-amyloidogenic pathway, are depicted. The endoplasmic reticulum membrane proteins reticulon 3 (RTN3) and reticulon 4 (RTN4) (arrows) are constant elements in all the stages and regions

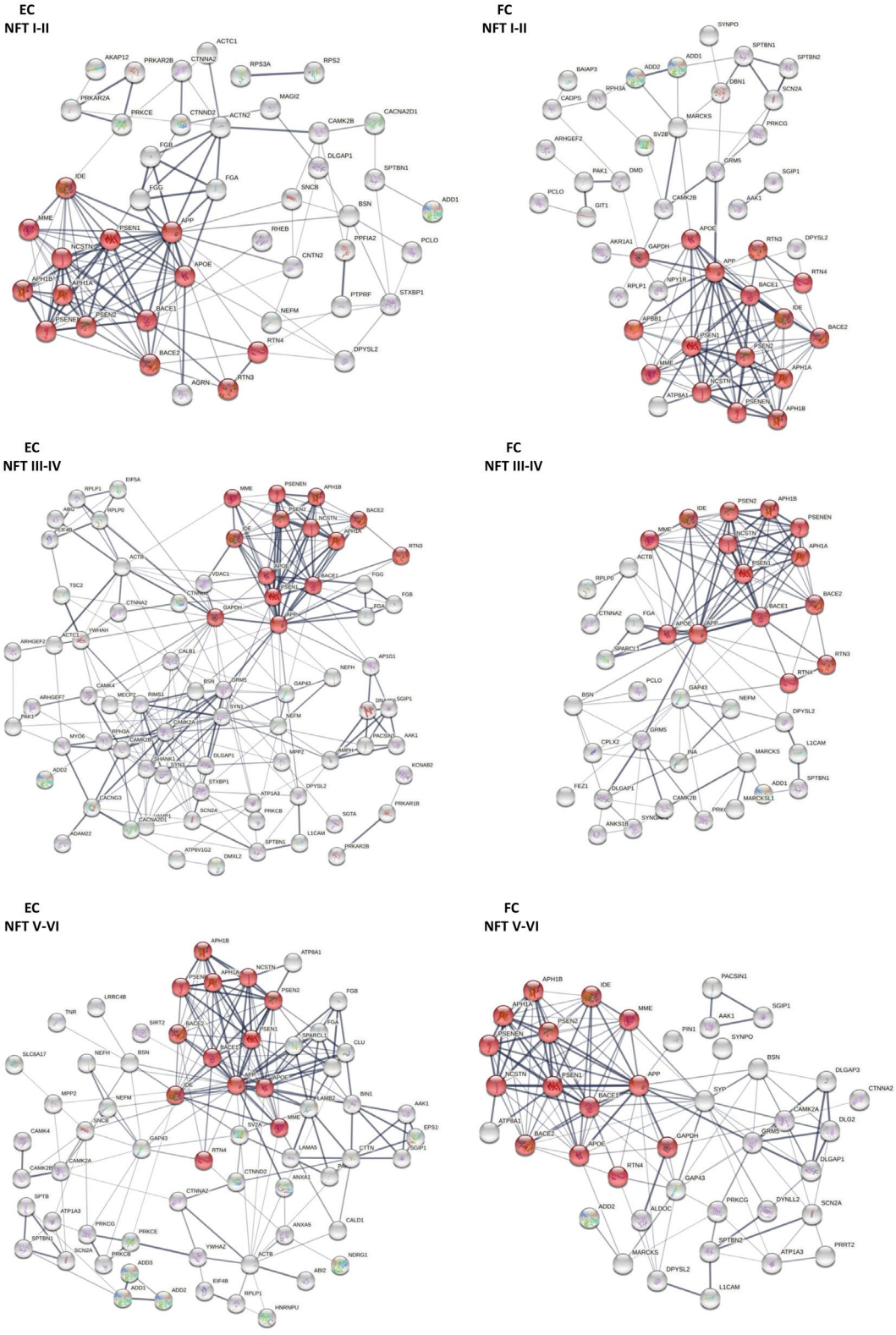

FIGURE 6 Functional interactomes of dysregulated synaptic proteins and phosphoproteins in the EC and FC at different stages of NFT pathology (stages I–II, III–IV, and V–VI of Braak). A large number of proteins are dysregulated at the first stages (I–II) in the EC and FC. Most dysregulation occurs in the middle stages (III–IV) of AD-related pathology. A small number of proteins are not shown because they do not interact with the proteins represented in the diagrams. Dysregulated proteins were artificially combined with proteins linked to β-amyloid formation (red balls), including β-amyloid precursor protein (APP), presenilin1 (PSEN1), presenilin 2 (PSEN2), β-secretase 1 (BACE1), BACE 2, apolipoprotein E (ApoE4), aph-1 homolog A γ-secretase subunit (APH1A), APH1B, nicastrin (NCT/NCSTN), presenilin enhancer γ-secretase subunit (PEN2/PSENEN), neprilysin (NEP/MME), and insulin-degrading enzyme (IDE)

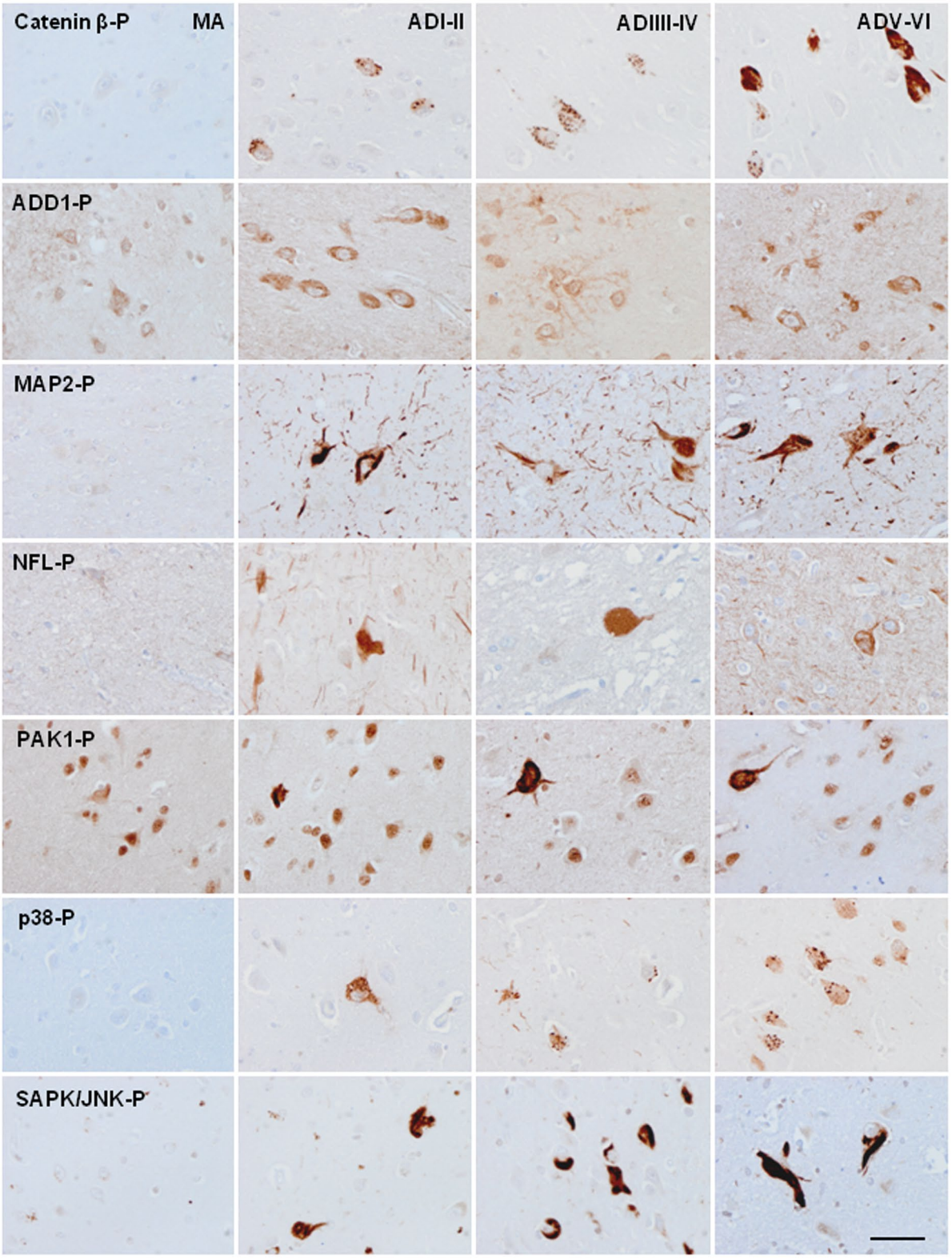

FIGURE 7 Immunohistochemistry of selected phosphorylated proteins in the EC at different stages of NFT pathology (stages I–II, III–IV, and V–VI of Braak). Phosphorylated catenin-β and p38-P immunoreactivity appear at the first and middle stages of NFT pathology as small granules in the cytoplasm of a subpopulation of neurons. This pattern is also found for p38-P in many neurons of the EC at stages V–VI of NFT pathology. MAP2-P, NFL-P, and SAPK/JNK-P immunoreactivity is found in neurons with the morphology of NFTs from the first stages onwards; the number of affected neurons increases with disease progression. The number of NFL-P-positive neurons is, by far, smaller than the number of neurons with MAP2-P pathology in consecutive sections. PAK1-P immunoreactivity is seen in NFTs at stages III–IV and V–VI, but as irregular or granular deposits in EC neurons at staged I–II. ADD1-P immunoreactivity increases in astrocytes and in a subpopulation of NFTs at middle and advanced stages of NFT pathology. Paraffin sections, lightly counterstained with hematoxylin, bar = 50 μm

4.1 | Comparison of previous and present phosphoproteomics studies in AD-related pathology

In the context of AD, pioneering studies identified a few abnormally phosphorylated proteins in the hippocampus and cerebral cortex in small numbers of cases with AD compared with controls (23, 24, 25, 27). Along with those studies, Rudrabhatla et al. (50) used iTRAQ-based phosphoproteomics in FC to identify all three phosphorylated neurofilament proteins associated with NFT in AD. Dammer et al. used IMAC coupled with LC-MS/MS to identify 253 phosphopeptides with elevated or decreased levels in the FC of eight AD cases compared with eight controls (post-mortem delay between 3 and 11 h) (29). In addition to tau, phosphopeptide levels were over-represented by proteins associated with the plasma membrane, glycoproteins, cytoskeletal binding, synapse, small heat shock proteins (HSP 27 and crystallin-αB), kinases, and alternative splicing. Interestingly, kinase activation linked to heat shock proteins was considered a pathogenic mechanism in AD.

Sathe et al. (30) used TMT along with IMAC to enrich phosphopeptides in order to examine the frontal gyrus of people with AD and age-matched cognitively normal subjects; 350 proteins were significantly altered in AD: 389 phosphopeptides increased whereas 115 phosphopeptides decreased phosphorylation. The categorization of altered proteins was based on a human protein reference database (HPRD) (52). Most of the altered phosphorylated proteins were localized in the cytoplasm (37%), followed by the nucleus (29%), plasma membrane (20%), and extracellular (8%) sites. The molecular function of abnormally phosphorylated proteins corresponds to adhesion molecules (17%), serine/threonine kinases (12%), transport/cargo proteins (7%), and structural proteins, integral membrane proteins, and others (24%), mostly involved in cell growth and/or maintenance, cell communication, and metabolism. Network biology showed several molecules involved in RNA processing and splicing, neurogenesis and neural development, and the metabotropic glutamate receptor 5 (GRM5) calcium-signaling pathway. The main concern with this impressive study is the selection made of control samples (n = 6) composed of cases with NFT pathology stages II, III, and IV (CERAD: 0–1), and AD cases (n = 11) including those with Braak stages III–VI (CERAD: 3). Therefore, we lack data about the alterations at early stages of AD-related pathology and the changes occurring with disease progression.

The present findings show widespread dysregulated protein phosphorylation with brain aging and NFT progression to sAD. Such alteration is stage- and region-dependent, but several proteins are common to the EC and FC, and many are dysregulated in two or more stages in a particular region. Consequently, there is a core group of dysregulated proteins throughout the progression of the biological process of "normal" versus "pathological" aging. Up- and down-regulation of different phosphorylation sites occur in a particular protein in a given stage. Multiple phosphorylation of regulatory proteins is common in physiological and pathological conditions (53-56).

Our results in advanced stages of sAD are similar to those already reported by others, particularly Dammer et al. (29), Sathe et al. (30), and Bai et al. (28). Several identified dysregulated phosphoproteins are common to all of them. The recognition of altered molecular pathways, as expressed in GO terms, is also similar in the studies mentioned and in our present observations. These commonalities support the robustness of our phosphoproteomics approach.

4.2 | Protein phosphorylation is altered at early stages of NFT pathology

The novelty of the present study is the analysis of the first stages of NFT pathology (stages I–II) when compared with MA individuals with no NFT pathology, and the continuity and evolution of these modifications with NFT progression.

It may be suggested that changes at the first stages of NFT pathology are linked to aging rather than to NFT pathology, because MA individuals are younger than those with NFT pathology restricted to the entorhinal and transentorhinal cortex (stages I–II). In the EC, we identified sixty-five dysregulated proteins at stages I–II; in the FC eighty-one phosphoproteins were dysregulated at stages I–II when compared with MA. Comparative analysis in the EC at different stages revealed 22 phosphoproteins common to the three stages, 10 phosphoproteins common to stages V–VI and I–II, and 10 phosphoproteins common to stages III–IV and I–II. In the FC, the comparative analysis between different stages revealed 21 phosphoproteins common to the three stages, 14 (phospho)proteins common to stages V–VI and I–II, and 15 phosphoproteins common to stages III–IV and I–II. It is worth noting that the involvement of the EC occurs at the first stages of NFT pathology according to Braak and Braak. However, the FC is not affected by NFTs until stages V–VI. Moreover, cases categorized as stages I–II in the present series did not have β-amyloid in the EC while only two of them had β-amyloid deposits in the FC. In short, dysregulated protein phosphorylation of selected proteins occurs in parallel to the appearance of NFTs in the EC but precedes the appearance of NFTs and SPs in the FC. These findings are in line with previous observations showing altered molecular pathways in the FC at early stages of AD-related pathology (14).

Tau is one of the many cytoskeletal proteins with altered phosphorylation at the early stages of aging and sAD. Although tau interacts with a large number of proteins (57), not all dysregulated phosphoproteins identified in the present study are functionally linked with tau, thus suggesting that selected dysregulated phosphorylation does not

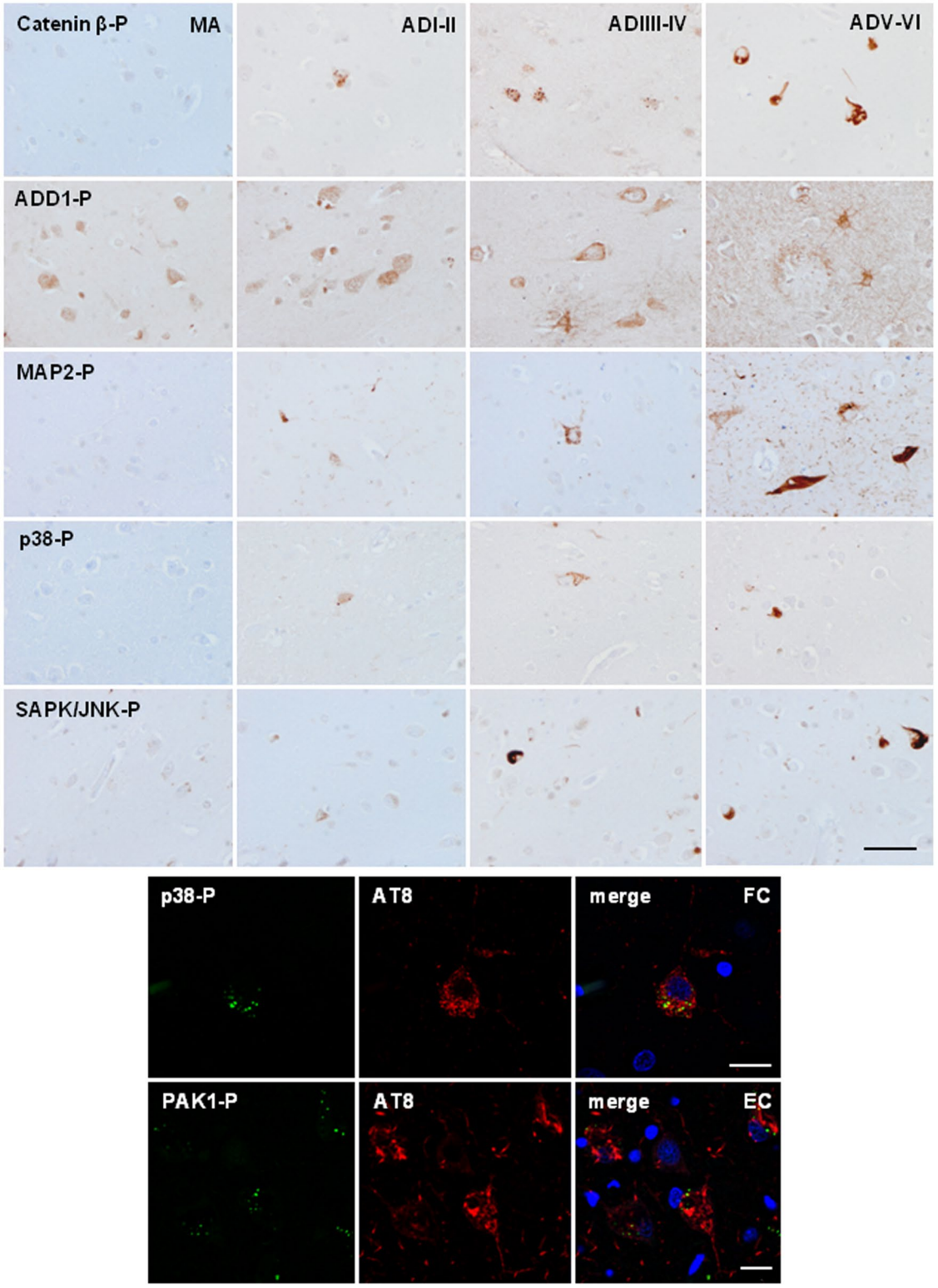

FIGURE 8 Upper panel: Immunohistochemistry of selected phosphorylated proteins in the FC at different stages of NFT pathology (stages I–II, III–IV, and V–VI of Braak). Phosphorylated catenin-β and p38-P immunoreactivity are found as small granules in the cytoplasm of very few neurons at the first and middle stages of NFT pathology. Catenin β-P decorates a few NFTs at stages V–VI, and p38-P is found in medium-sized neuronal inclusions in a subpopulation of neurons. A few cortical neurons show MAP2-P and SAPK-JNK-P-immunoreactive deposits at stages I–II and III–IV. NFTs are stained with MAP2-P and SAPK/JNK-P antibodies at stages V–VI. ADD1-P immunoreactivity is increased in the cytoplasm and processes of astrocytes, and the cytoplasm of a subpopulation of neurons at the middle and advanced stages of the disease. Paraffin sections lightly counterstained with hematoxylin, bar = 50 μm. Lower panel: Double-labeling immunofluorescence and confocal microscopy of p38-P (green) and AT8 (red) in the FC at stages III–IV, and PAK1-P (green) and AT8 (red) in the EC at stages I–II. p38-P is found as small granules in neurons with early phospho-tau deposits; PAK1-P is found as small granules in neurons at different stages of phospho-tau deposition including pre-tangles and tangles. Nuclei are labeled with DRAQ5^{TM} (blue). Paraffin sections, bar = 20 μm

necessarily depend on the abnormal phosphorylation state of tau.

Considering the total number of identified dysregulated phosphoproteins, the most active period corresponds to stages III–IV, at the time when a subpopulation of people might be clinically categorized as suffering from a mild cognitive impairment which is a preceding determinant stage in the progression to dementia.

4.3 | Categorization of dysregulated phosphoproteins and implications in brain function

The main group of dysregulated phosphoproteins is composed of membrane proteins, proteins of the cytoskeleton, proteins of the synapses and dense core vesicles, and proteins linked to membrane transport and ion channels, accounting for a total of 141 proteins. Thirty-six proteins are abnormally phosphorylated in the EC at stage I–II while forty-seven proteins are abnormally phosphorylated in the FC at stage I–II. Proteins categorized as kinases, proteins linked to DNA or protein deacetylation, proteins linked to gene transcription and protein synthesis, and proteins involved in energy metabolism form a second instrumental group. Nineteen proteins, including nine kinases, are abnormally phosphorylated in the EC at stages I–II of NFT pathology compared with MA. Twenty-five dysregulated phosphoproteins are identified in the FC at stages I–II; six are kinases.

Analyzing the functional implications of dysregulated protein phosphorylation of such a large number of proteins is not an easy task. Bioinformatics approaches such as GO terms of biological function are useful as instruments, but a list of GO terms is often, as in the present scenario, overwhelming. Moreover, the functional consequences of altered phosphorylation, particularly those involving hyper- and hypophosphorylation in different sites of the protein at a given time, are not known. Since the functional consequences of altered tau phosphorylation have been extensively studied, this point will not be discussed. For these reasons, only a few of the selected groups of proteins such as kinases, proteins of the synapses, and the amyloidogenic pathway are discussed here in greater detail. Thus, twenty four kinases are abnormally phosphorylated across NFT staging in the EC and FC. However, this is an underrepresentative number, as other kinases were not recognized in our (phospho)proteomics study. p38-P and SAPK/JNK-P are expressed in selected EC and FC neurons in all the stages of NFT pathology. Immunohistochemistry and double-labeling immunofluorescence and confocal microscopy reveal phosphorylated p38 as small cytoplasmic granules in neurons with small deposits of P-tau; only at advanced stages is p38-P incorporated in a subpopulation of NFTs. SAPK/JNK-P immunoreactivity co-localizes with NFTs in the EC at stages I–II, but it is only at stages III–IV that phosphorylated SAPK/JNK accompanies small deposits of P-tau in the FC. Therefore, early and persistent activation of kinases appears to play a crucial role in the dysregulated phosphorylation of proteins in brain aging and sAD.

Synaptic pathology is a decisive substrate of cognitive impairment and dementia in AD (58-61). Most studies are focused on the deleterious effects of soluble toxic forms of β-amyloid and tau at the synapses (62-65). Oxidative stress damage, inflammation, and epigenetic and signal transduction alterations are involved as well (66-69). Previous studies in four mouse models of AD showed a connection between early β-amyloid deposition in the brain and phosphorylation of proteins linked to synaptic spine formation. Systems biology analyses suggested that phosphorylation of myristoylated alanine-rich C kinase substrate MARCKS by overactivated kinases including protein kinases C and calmodulin-dependent kinases initiated synapse pathology (70). The present study identifies MARCKs phosphorylation and activation of several different types of CAMKs and PKCs, some of them at the first stages of NFT pathology; this occurs in parallel to dysregulated phosphorylation of synaptic proteins in the FC and EC at different stages of NFT pathology, some of it before the appearance of β-amyloid deposits in FC and EC.

Phosphorylation of selected membrane proteins also has an impact on the amyloidogenic pathway. APP is phosphorylated in AD, and its phosphorylation at specific sites promotes APP processing and facilitates β-amyloid production (71-73). The possibility that changes in the phosphorylation of other membrane proteins also interfere with the amyloidogenic pathway of APP degradation is suggested by analysis of interactomes of APP-related proteins and selected membrane proteins. Among these, RTN3 and RTN4/NOGO-B interact with BACE1 and reduce the production of β-amyloid and the amount of β-amyloid plaques (74-76). According to PhosphoSitePlus database, RTN3 and RTN4 have more than twenty phosphorylation sites across the amino acid sequence. However, little is known about the consequences of RTN3 and RTN4 hypophosphorylation and its functional effects on BACE1 and other putative interactors, as it occurs in the EC and FC at the middle stages of NFT pathology. As a working hypothesis, altered phosphorylation of RTN3 and RTN4 may modulate the β-amyloidogenic pathway, thus contributing to SP formation.

4.4 | Is there a link between lipid microdomains at the cell membrane, diacylglycerol, and altered protein phosphorylation?

Lipid rafts are microdomains of the plasma membrane, enriched in gangliosides, glycosphingolipids, and cholesterol.

Lipid rafts facilitate communication between extracellular stimuli and the intracellular milieu through ion channels and a variety of signaling receptors; moreover, membrane proteins and components of the cytoskeleton anchor in and bind to lipid rafts and regulate receptor activation, signaling pathways, and cellular polarity (77). The lipid composition of lipid rafts is altered in aging and more dramatically in AD (78-81). Experimental pieces of evidence point to the facilitation of β-amyloid production linked to the abnormalities in the lipid raft composition in lipid rafts in AD (82-84). The present observations showing altered phosphorylation of proteins linked to the cell membrane, membrane signaling, cytoskeleton and synapses, lead to thinking about enhancer complementary unfavourable effects of lipids and proteins at the level of cell membrane/cytoskeleton signaling in aging and AD.

It is also worth considering as a working hypothesis that dysregulated phosphoproteins, including tau and β-amyloid, converge and point to alterations in the diacylglycerol-mediated signaling pathway. Diacylglycerol (DAG) has unique functions as a constituent of cell membranes, intermediate lipid metabolism, and a key component in lipid-mediated signalling (85, 86). In neurons, DAG modulates several signal transduction proteins (87), which, in turn, are linked to the activation of ion channels, protein kinases, traffic and fusion of synaptic vesicles, axonal guidance, and cytoskeletal homeostasis, among others (85, 87, 88). Significantly, tau and β-amyloid phosphorylation may also be mediated by diacylglycerols and protein kinase C (89, 90). Levels of glycerophospholipids, sphingolipids, and DAGs are altered in the brain in AD (91). Specifically, the most unique and consistent finding of these lipidomics studies is the increase of DAG levels in the AD frontal cortex (92,93). Further studies are needed to learn about the function of DAG in protein phosphorylation in AD.

4.5 | Final considerations

The present findings provide a comprehensive reconstruction of altered protein phosphorylation in the FC and EC, which is line with previous observations at advanced stages of AD, and provides for the first time robust data on the first and middle stages of NFT pathology linked to AD. It must be stressed that phosphoproteomics has limitations regarding the capacity to recognize the totality of phosphoproteins in a given sample and the thresholds used to consider an abnormally regulated phosphoprotein. This may explain why some proteins appear to be abnormally regulated at stages I–II and V–VI but are apparently normal at stages III–IV, at the time that the same protein is abnormally hyperphosphorylated through NFT progression when assessed with immunohistochemistry using phospho-specific antibodies.

We do not know to what extent dysregulated protein phosphorylation contributes to degeneration in aging and sAD, but it may be hypothesized that the impressive involvement of proteins of membranes, synapses, and cytoskeleton, together with altered activation of several kinases, impairs brain function and contributes to abnormal membrane signal transduction, synaptic transmission, β-amyloid processing, and axonal and membrane transport. The key point of the present work is the demonstration that dysregulated protein phosphorylation occurs at the first stages of NFT pathology, linking brain aging to sAD. Even considering the plastic capacity of the nervous system, altered phosphorylation of crucial brain proteins foreshadows impaired brain function that may underlie cognitive deficits interpreted as normal brain aging in individuals at the first and middle stages of NFT pathology.

ACKNOWLEDGMENTS

We wish to thank Tom Yohannan for editorial help.

CONFLICT OF INTEREST

No relevant data.

AUTHOR CONTRIBUTIONS

Isidro Ferrer and Enrique Santamaría designed the study; Pol Andrés-Benito selected the tissue samples and performed immunohistochemistry; Joaquín Fernández-Irigoyen, Karina Ausín, and Enrique Santamaría performed the proteomic analysis; Isidro Ferrer, José Antonio del Rio, Karina Ausín, Joaquín Fernández-Irigoyen, and Enrique Santamaría analyzed and interpreted the data; Reinald Pamplona discussed the role of lipids; Isidro Ferrer and Enrique Santamaría wrote the manuscript. All authors critically revised the manuscript.

DATA AVAILABILITY STATEMENT

All data generated or analyzed during this study are included in this published article and its Supporting Information files; to the ProteomeXchange Consortium (http://proteomecentral.proteomexchange.org) via the PRIDE partner repository with the dataset identifiers PXD021645 (Reviewer account details: Username: reviewer_pxd021645@ebi.ac.uk; Password: ANBskoaI) and PXD021653 (Reviewer account details: Username: reviewer_pxd021653@ebi.ac.uk; Password: kMAyoOkq).

ETHICS APPROVAL AND CONSENT TO PARTICIPATE

Post-mortem samples were obtained from the Institute of Neuropathology HUB-ICO-IDIBELL Biobank following the guidelines of Spanish legislation on this matter and the approval of the CEIC of the Bellvitge University Hospital.

ORCID

Isidro Ferrer https://orcid.org/0000-0001-9888-8754
Pol Andrés-Benito https://orcid.org/0000-0003-3000-0338
Joaquín Fernández-Irigoyen https://orcid.org/0000-0001-5072-4099
Enrique Santamaría https://orcid.org/0000-0001-8046-8102

REFERENCES

1. Braak H, Del Tredici K. The pathological process underlying Alzheimer's disease in individuals under thirty. Acta Neuropathol. 2011;121:171–81. https://doi.org/10.1007/s00401-010-0789-4
2. Goedert M, Wischik CM, Crowther RA, Walker JE, Klug A. Cloning and sequencing of the cDNA encoding a core protein of the paired helical filament of Alzheimer disease: identification as microtubule-associated protein tau. Proc Natl Acad Sci U S A. 1988;85:4051–5. https://doi.org/10.1073/pnas.85.11.4051
3. Goedert M, Spillantini MG, Cairns NJ, Crowther RA. Tau proteins in Alzheimer paired helical filaments: abnormal phosphorylation of all six brain isoforms. Neuron. 1992;8:159–68. https://doi.org/10.1016/0896-6273(92)90117-v
4. Buée L, Bussière T, Buée-Scherrer V, Delacourte A, Hof PR. Tau protein isoforms, phosphorylation, and role in neurodegenerative disorders. Brain Res Brain Res Rev. 2000;33:95–130. https://doi.org/10.1016/s0165-0173(00)00019-9
5. Hernández F, Avila J. Tauopathies. Cell Mol Life Sci. 2007;64:2219–33. https://doi.org/10.1007/s00018-007-7220-x
6. Iqbal K, del C. Alonso A, Chen S, Chohan MO, El-Akkad E, Gong CX, et al. Tau pathology in Alzheimer disease and other tauopathies. Biochim Biophys Acta. 2005;1739:198–210. https://doi.org/10.1016/j.bbadis.2004.09.008
7. Spillantini MG, Goedert M. Tau pathology and neurodegeneration. Lancet Neurol. 2013;12:609–22. https://doi.org/10.1016/s0166-2236(98)01337-x
8. Braak H, Braak E. Neuropathological staging of Alzheimer-related changes. Acta Neuropathol. 1991;82:239–59. https://doi.org/10.1007/BF00308809
9. Braak H, Braak E. Staging of Alzheimer's disease-related neurofibrillary changes. Neurobiol Aging. 1995;16:271–8. https://doi.org/10.1016/0197-4580(95)00021-6
10. Braak H, Thal DR, Ghebremedhin E, Del Tredici K. Stages of the pathologic process in Alzheimer disease: age categories from 1 to 100 years. J Neuropathol Exp Neurol. 2011;70:960–9. https://doi.org/10.1097/NEN.0b013e318232a379
11. Dubois B, Hampel H, Feldman HH, Scheltens P, Aisen P, Andrieu S, et al. Preclinical Alzheimer's disease: definition, natural history, and diagnostic criteria. Alzheimers Dement. 2016;12:292–323. https://doi.org/10.1016/j.jalz.2016.02.002
12. Nelson PT, Alafuzoff I, Bigio EH, Bouras C, Braak H, Cairns NJ, et al. Correlation of Alzheimer disease neuropathologic changes with cognitive status: a review of the literature. J Neuropathol Exp Neurol. 2012;71:362–81. https://doi.org/10.1097/NEN.0b013e31825018f7
13. Braak H, Braak E. Frequency of stages of Alzheimer-related lesions in different age categories. Neurobiol Aging. 1997;18:351–7. https://doi.org/10.1016/s0197-4580(97)00056-0
14. Ferrer I. Defining Alzheimer as a common age-related neurodegenerative process not inevitably leading to dementia. Prog Neurogibol. 2012;97:38–51. https://doi.org/10.1016/j.pneurobio.2012.03.005
15. Ferrer I, Andrés-Benito P. White matter alterations in Alzheimer's disease without concomitant pathologies. Neuropathol Appl Neurobiol. 2020;46:654–72. https://doi.org/10.1111/nan.12618
16. Aisen PS, Cummings J, Jack CR, Morris CJ, Sperling R, Frölich L, et al. On the path to 2025: understanding the Alzheimer's disease continuum. Alzheimers Res Ther. 2017;9:60. https://doi.org/10.1186/s13195-017-0283-5
17. Braak H, Del Tredici K. The preclinical phase of the pathological process underlying sporadic Alzheimer's disease. Brain. 2015;138:2814–33. https://doi.org/10.1093/brain/awv236
18. Karlawish J, Jack CR, Rocca WA, Snyder HM, Carrillo MC. Alzheimer's disease: The next frontier-Special Report 2017. Alzheimers Dement. 2017;13:374–80. https://doi.org/10.1016/j.jalz.2017.02.006
19. Crary JF, Trojanowski JQ, Schneider JA, Abisambra JF, Abner EL, Alafuzoff I, et al. Primary age-related tauopathy (PART): a common pathology associated with human aging. Acta Neuropathol. 2014;128:755–66. https://doi.org/10.1007/s00401-014-1349-0
20. Bell WR, An Y, Kageyama Y, English C, Rudow GL, Pletnikova O, et al. Neuropathologic, genetic, and longitudinal cognitive profiles in primary age-related tauopathy (PART) and Alzheimer's disease. Alzheimers Dement. 2019;15:8–16. https://doi.org/10.1016/j.jalz.2018.07.215
21. Duyckaerts C, Braak H, Brion JP, Buée L, Del Tredici K, Goedert M, et al. PART is part of Alzheimer disease. Acta Neuropathol. 2015;129:749–56. https://doi.org/10.1007/s00401-015-1390-7
22. McMillan CT, Lee EB, Jefferson-George K, Naj A, Van Deerlin VM, Trojanowski JQ, et al. Alzheimer's genetic risk is reduced in primary age-related tauopathy: a potential model of resistance? Annals of Clin Transl Neurol. 2018;5:927–34. https://doi.org/10.1002/acn3.581
23. Di Domenico F, Sultana R, Barone E, Perluigi M, Cini C, Mancuso C, et al. Quantitative proteomics analysis of phosphorylated proteins in the hippocampus of Alzheimer's disease subjects. J Proteome. 2011;74:1091–103. https://doi.org/10.1016/j.jprot.2011.03.033
24. Tan H, Wu Z, Wang H, Bai B, Li Y, Wang X, et al. Refined phosphopeptide enrichment by phosphate additive and the analysis of human brain phosphoproteome. Proteomics. 2015;15:500–7. https://doi.org/10.1002/pmic.201400171
25. Triplett JC, Swomley AM, Cai J, Klein JB, Butterfield DA. Quantitative phosphoproteomic analyses of the inferior parietal lobule from three different pathological stages of Alzheimer's disease. J Alzheimers Dis. 2016;49:45–62. https://doi.org/10.3233/JAD-150417
26. Xia Q, Cheng D, Duong DM, Gearing M, Lah JJ, Levy AI, et al. Phosphoproteomic analysis of human brain by calcium phosphate precipitation and mass spectrometry. J Proteome Res. 2008;7:2845–51. https://doi.org/10.1021/pr8000496
27. Zahid S, Oellerich M, Asif AR, Ahmed N. Phosphoproteome profiling of substantia nigra and cortex regions of Alzheimer's disease patients. J Neurochem. 2012;121:954–63. https://doi.org/10.1111/j.1471-4159.2012.07737.x
28. Bai B, Wang X, Li Y, Chen PC, Yu K, Dey KK, et al. Deep multilayer brain proteomics identifies molecular networks in Alzheimer's disease progression. Neuron. 2020;105:975–91.e7. https://doi.org/10.1016/j.neuron.2019.12.015
29. Dammer EB, Lee AK, Duong DM, Gearing M, Lah JJ, Levey AI, et al. Quantitative phosphoproteomics of Alzheimer's disease reveals cross-talk between kinases and small heat shock proteins. Proteomics. 2015;15:508–19. https://doi.org/10.1002/pmic.201400189
30. Sathe G, Mangalaparthi KK, Jain A, Darrow J, Troncoso J, Albert M, et al. Multiplexed phosphoproteomic study of the brain in patients with Alzheimer's disease and age-matched cognitively healthy controls. OMICS. 2020;24:2016–227. https://doi.org/10.1089/omi.2019.0191
31. Ferrer I. Brain banking. In: Aminoff MJ, Daroff RB, eds. Encyclopedia of the neurological sciences, 2nd ed. vol. 1. Academic Press; 2014:467–73.

32. Braak H, Alafuzoff I, Arzberger T, Kretzschmar H, Del Tredici K. Staging of Alzheimer disease-associated neurofibrillary pathology using paraffin sections and immunocytochemistry. Acta Neuropathol. 2006;112:389–404. https://doi.org/10.1007/s00401-006-0127-z
33. Thal DR, Rüb U, Orantes M, Braak H. Phases of A beta-deposition in the human brain and its relevance for the development of AD. Neurology. 2002;58:1791–800. https://doi.org/10.1212/wnl.58.12.1791
34. Hyman BT, Phelps CH, Beach TG, Bigio EH, Cairns NJ, Carrillo MC, et al. National Institute on Aging-Alzheimer's Association guidelines for the neuropathologic assessment of Alzheimer's disease. Alzheimers Dement. 2012;8:1–13. https://doi.org/10.1016/j.jalz.2011.10.007
35. Montine TJ, Phelps CH, Beach TG, Bigio EH, Cairns NJ, Dickson DW, et al. National Institute on Aging-Alzheimer's Association guidelines for the neuropathologic assessment of Alzheimer's disease: a practical approach. Acta Neuropathol. 2012;123:1–11. https://doi.org/10.1007/s00401-011-0910-3
36. Montoya A, Beltran L, Casado P, Rodríguez-Prados JC, Cutillas PR. Characterization of a TiO_2 enrichment method for label-free quantitative phosphoproteomics. Methods. 2011;54:370–8. https://doi.org/10.1016/j.ymeth.2011.02.004
37. Collins BC, Hunter CL, Liu Y, Schilling B, Rosenberger G, Bader SL, et al. Multi-laboratory assessment of reproducibility, qualitative and quantitative performance of SWATH-mass spectrometry. Nat Commun. 2017;8:291. https://doi.org/10.1038/s41467-017-00249-5
38. Shevchenko A, Tomas H, Havli J, Olsen JV, Mann M. In-gel digestion for mass spectrometric characterization of proteins and proteomes. Nat Protoc. 2006;1:2856–60. https://doi.org/10.1038/nprot.2006.468
39. Shilov IV, Seymour SL, Patel AA, Loboda A, Tang WH, Sean P, et al. The paragon algorithm, a next-generation search engine that uses sequence temperature values and features probabilities to identify peptides from tandem mass spectra. Mol Cel Proteom. 2007;6:1638–55. https://doi.org/10.1074/mcp.T600050-MCP200
40. Tang WH, Shilov IV, Seymour SL. Nonlinear fitting method for determining local false discovery rates from decoy database searches. J Proteome Res. 2008;7:3661–7. https://doi.org/10.1021/pr070492f
41. Gillet LC, Navarro P, Tate S, Röst H, Selevsek N, Reiter L, et al. MetDIA: targeted data extraction of the MS/MS spectra generated by data-independent acquisition: a new concept for consistent and accurate proteome analysis. Mol Cel Proteom. 2012;11:O111.016717. https://doi.org/10.1021/acs.analchem.6b02122
42. Zhou Y, Zhou B, Pache L, Chang M, Khodabakhshi AH, Tanaseichuk O, et al. Metascape provides a biologist-oriented resource for the analysis of systems-level datasets. Nat Commun. 2019;10:1523. https://doi.org/10.1038/s41467-019-09234-6
43. Szklarczyk D, Franceschini A, Wyder S, Forslund K, Heller D, Huerta-Cepas J, et al. STRING v10: protein-protein interaction networks, integrated over the tree of life. Nucleic Acids Res. 2015;43:D447–52. https://doi.org/10.1093/nar/gku1003
44. Masters CL, Beyreuther K. Amyloid-β production. In: Dickson DW, Weller RO, eds. Neurodegeneration: the molecular pathology of dementia and movement disorders, 2nd ed. Blackwell Publishing Co; 2011:92–6.
45. Koopmans F, van Nierop P, Andres-Alonso M, Byrnes A, Cijsouw T, Coba MP, et al. SynGO: An evidence-based, expert-curated knowledge base for the synapse. Neuron. 2019;103:217–234.e4. https://doi.org/10.1016/j.neuron.2019.05.002
46. Atzori C, Ghetti B, Piva R, Srinivasan AN, Zolo P, Delisle MB, et al. Activation of the JNK/p38 pathway occurs in diseases characterized by tau protein pathology and is related to tau phosphorylation but not to apoptosis. J Neuropathol Exp Neurol. 2001;60:1190–7. https://doi.org/10.1093/jnen/60.12.1190
47. Ferrer I, Blanco R, Carmona M, Puig B. Phosphorylated mitogen-activated protein kinase (MAPK/ERK-P), protein kinase of 38 kDa (p38-P), stress-activated protein kinase (SAPK/JNK-P), and calcium/calmodulin-dependent kinase II (Cam kinase II) are differentially expressed in tau deposits in neurons and glial cells in tauopathies. J Neural Transm. 2001;108:1397–415. https://doi.org/10.1007/s007020100016
48. Ferrer I, Gomez-Isla T, Puig B, Freixes M, Ribé E, Dalfó E, et al. Current advances on different kinases involved in tau phosphorylation in Alzheimer's disease and tauopathies. Curr Alzheimer Res. 2005;2:3–18. https://doi.org/10.2174/1567205052772713
49. Haugh MC, Probst A, Ulrich J, Kahn J, Anderton BH. Alzheimer neurofibrillary tangles contain phosphorylated and hidden neurofilament epitopes. J Neurol Neurosurg Psychiatry. 1986;49:1213–20. https://doi.org/10.1136/jnnp.49.11.1213
50. Rudrabhatla P, Jaffe H, Pant HC. Direct evidence of phosphorylated neuronal intermediate filament proteins in neurofibrillary tangles (NFTs): phosphoproteomics of Alzheimer's NFTs. FASEB J. 2011;25:3896–905. https://doi.org/10.1096/fj.11-181297
51. Paraizo Leite RE, Grinberg LT. Closing the gap between brain banks and proteomics to advance the study of neurodegenerative diseases. Proteomics Clin Appl. 2015;9:832–7. https://doi.org/10.1002/prca.201400192
52. Prasad TS, Kandasamy K, Pandey A. Human protein reference database and human proteinpedia as discovery tools for systems biology. Methods Mol Biol. 2009;577:67–79. https://doi.org/10.1007/978-1-60761-232-2_6
53. Cohen P. The regulation of protein function by multisite phosphorylation–a 25 year update. Trends Biochem Sci. 2000;25:596–601. https://doi.org/10.1016/s0968-0004(00)01712-6
54. Kapuy O, Barik D, Domingo Sananes MR, Tyson JJ, Novák B. Bistability by multiple phosphorylation of regulatory proteins. Prog Biophys Mol Biol. 2009;100:47–56. https://doi.org/10.1016/j.pbiomolbio.2009.06.004
55. Salazar C, Höfer T. Multisite protein phosphorylation–from molecular mechanisms to kinetic models. FEBS J. 2009;276:3177–98. https://doi.org/10.1111/j.1742-4658.2009.07027.x
56. Varedi K SM, Ventura AC, Merajver SD, Lin XN. Multisite phosphorylation provides an effective and flexible mechanism for switch-like protein degradation. PLoS One. 2010;5:e14029. https://doi.org/10.1371/journal.pone.0014029
57. Drummond E, Pires G, MacMurray C, Askenazi M, Nayak S, Bourdon M, et al. Phosphorylated tau interactome in the human Alzheimer's disease brain. Brain. 2020;143:2803–17. https://doi.org/10.1093/brain/awaa223
58. DeKosky S, Scheff S. Synapse loss in frontal cortex biopsies in Alzheimer's disease: correlation with cognitive severity. Ann Neurol. 1990;27:457–64. https://doi.org/10.1002/ana.410270502
59. Masliah E, Mallory M, Hansen L, DeTeresa R, Alford M, Terry R. Synaptic and neuritic alterations during the progression of Alzheimer's disease. Neurosci Lett. 1994;174:67–72. https://doi.org/10.1016/0304-3940(94)90121-x
60. Selkoe DJ. Alzheimer's disease is a synaptic failure. Science. 2002;298:789–91. https://doi.org/10.1126/science.1074069
61. Terry RD, Masliah E, Salmon DP, Butters N, DeTeresa R, Hill R, et al. Physical basis of cognitive alterations in Alzheimer's disease: synapse loss is the major correlate of cognitive impairment. Ann Neurol. 1991;30:572–80. https://doi.org/10.1002/ana.410300410
62. Dourlen P, Kilinc D, Malmanche N, Chapuis J, Lambert JC. The new genetic landscape of Alzheimer's disease: from amyloid cascade to genetically driven synaptic failure hypothesis? Acta Neuropathol. 2019;138:221–36. https://doi.org/10.1007/s00401-019-02004-0
63. Gouras GK, Tampellini D, Takahashi RH, Capetillo-Zarate E. Intraneuronal beta-amyloid accumulation and synapse pathology in Alzheimer's disease. Acta Neuropathol. 2010;119:523–41. https://doi.org/10.1007/s00401-010-0679-9

64. Palop JJ, Mucke L. Amyloid beta-induced neuronal dysfunction in Alzheimer's disease: from synapses toward neural networks. Nat Neurosci. 2010;13:812–8. https://doi.org/10.1038/nn.2583
65. Spires-Jones TL, Hyman BT. The intersection of amyloid-beta and tau at synapses in Alzheimer's disease. Neuron. 2014;82:756–71. https://doi.org/10.1016/j.neuron.2014.05.004
66. Briggs CA, Chakroborty S, Stutzmann GE. Emerging pathways driving early synaptic pathology in Alzheimer's disease. Biochem Biophys Res Commun. 2017;483:988–97. https://doi.org/10.1016/j.bbrc.2016.09.088
67. Jiang S, Bhaskar K. Dynamics of the complement, cytokine, and chemokine systems in the regulation of synaptic function and dysfunction relevant to Alzheimer's disease. J Alzheimers Dis. 2017;57:1123–35. https://doi.org/10.3233/JAD-161123
68. Kamat PK, Kalani A, Rai S, Swarnkar S, Tota S, Nath C, et al. Mechanism of oxidative stress and synapse dysfunction in the pathogenesis of Alzheimer's disease: understanding the therapeutic strategies. Mol Neurobiol. 2016;53:648–61. https://doi.org/10.1007/s12035-014-9053-6
69. Li K, Wei Q, Liu FF, Hu F, Xie AJ, Zhu LQ, et al. Synaptic dysfunction in Alzheimer's disease: Aβ, tau, and epigenetic alterations. Mol Neurobiol. 2018;55:3021–32. https://doi.org/10.1007/s12035-017-0533-3
70. Tagawa K, Homma H, Saito A, Fujita K, Chen X, Imoto S, et al. Comprehensive phosphoproteome analysis unravels the core signaling network that initiates the earliest synapse pathology in preclinical Alzheimer's disease brain. Hum Mol Genet. 2015;24:540–58. https://doi.org/10.1093/hmg/ddu475
71. Lee MS, Kao SC, Lemere CA, Xia W, Tseng HC, Zhou Y, et al. APP processing is regulated by cytoplasmic phosphorylation. J Cell Biol. 2013;163:83–95. https://doi.org/10.1083/jcb.200301115
72. Suzuki T, Nakaya T. Regulation of amyloid beta-protein precursor by phosphorylation and protein interactions. J Biol Chem. 2008;283:29633–7. https://doi.org/10.1074/jbc.R800003200
73. Vingtdeux V, Hamdane M, Gompel M, Bégard S, Drobecq H, Ghestem A, et al. Phosphorylation of amyloid precursor carboxy-terminal fragments enhances their processing by a gamma-secretase-dependent mechanism. Neurobiol Dis. 2005;20:625–37. https://doi.org/10.1016/j.nbd.2005.05.004
74. He W, Lu Y, Qahwash I, Hu XY, Chang A, Yan R. Reticulon family members modulate BACE1 activity and amyloid-beta peptide generation. Nat Med. 2004;10:959–65. https://doi.org/10.1038/nm1088
75. Murayama KS, Kametani F, Saito S, Kume H, Akiyama H, Araki W. Reticulons RTN3 and RTN4-B/C interact with BACE1 and inhibit its ability to produce amyloid beta-protein. Eur J Neurosci. 2006;24:1237–44. https://doi.org/10.1111/j.1460-9568.2006.05005.x
76. Shi Q, Ge Y, Sharoar MG, He W, Xiang R, Zhang Z, et al. Impact of RTN3 deficiency on expression of BACE1 and amyloid deposition. J Neurosci. 2014;34:13954–62. https://doi.org/10.1523/JNEUROSCI.1588-14.2014
77. Head BP, Patel HH, Insel PA. Interaction of membrane/lipid rafts with the cytoskeleton: impact on signaling and function: membrane/lipid rafts, mediators of cytoskeletal arrangement and cell signalling. Biochim Biophys Acta. 2014;1838:532–45. https://doi.org/10.1016/j.bbamem.2013.07.018
78. Díaz M, Fabelo N, Ferrer I, Marín R. "Lipid raft aging" in the human frontal cortex during nonpathological aging: gender influences and potential implications in Alzheimer's disease. Neurobiol Aging. 2018;67:42–52. https://doi.org/10.1016/j.neurobiolaging.2018.02.022
79. Fabelo N, Martín V, Marín R, Moreno D, Ferrer I, Díaz M. Altered lipid composition in cortical lipid rafts occurs at early stages of sporadic Alzheimer's disease and facilitates APP/BACE1 interactions. Neurobiol Aging. 2014;35:1801–12. https://doi.org/10.1016/j.neurobiolaging.2014.02.005
80. Fabelo N, Martín V, Marín R, Santpere G, Aso E, Ferrer I, et al. Evidence for premature lipid raft aging in APP/PS1 double-transgenic mice, a model of familial Alzheimer disease. J Neuropathol Exp Neurol. 2012;71:868–81. https://doi.org/10.1097/NEN.0b013e31826be03c
81. Martín V, Fabelo N, Santpere G, Puig B, Marín R, Ferrer I, et al. Lipid alterations in lipid rafts from Alzheimer's disease human brain cortex. J Alzheimers Dis. 2010;19:489–502. https://doi.org/10.3233/JAD-2010-1242
82. Díaz M, Fabelo N, Martín V, Ferrer I, Gómez T, Marín R. Biophysical alterations in lipid rafts from human cerebral cortex associate with increased BACE1/AβPP interaction in early stages of Alzheimer's disease. J Alzheimers Dis. 2015;43:1185–98. https://doi.org/10.3233/JAD-141146
83. Fabiani C, Antonillini SS. Alzheimer's disease as a membrane disorder: spatial cross-talk among β-amyloid peptides, nicotinic acetylcholine receptors and lipid rafts. Front Cell Neurosci. 2019;13:309. https://doi.org/10.3389/fncel.2019.00309
84. Vetrivel KS, Thinakaran G. Membrane rafts in Alzheimer's disease beta-amyloid production. Biochim Biophys Acta. 2010;1801:860–7. https://doi.org/10.1016/j.bbalip.2010.03.007
85. Almena M, Mérida I. Shaping up the membrane: diacylglycerol coordinates spatial orientation of signalling. Trends Biochem Sci. 2011;36:593–603. https://doi.org/10.1016/j.tibs.2011.06.005
86. Carrasco S, Mérida I. Diacylglycerol, when simplicity becomes complex. Trends Biochem Sci. 2007;32:27–36. https://doi.org/10.1016/j.tibs.2006.11.004
87. Sakane F, Hoshino F, Murakami C. New era of diacylglycerol kinase, phosphatidic acid and phosphatidic acid-binding protein. Int J Mol Sci. 2020;21:6794. https://doi.org/10.3390/ijms21186794
88. Mérida I, Ávila-Flores A, Merino E. Diacylglycerol kinases: at the hub of cell signalling. Biochem J. 2008;409:1–18.
89. Ekinci FJ, Shea TB. Free PKC catalytic subunits (PKM) phosphorylate tau via a pathway distinct from that utilized by intact PKC. Brain Res. 1999;850:207–16. https://doi.org/10.1016/s0006-8993(99)02146-0
90. Lee RK, Jimenez JJ, Cox AJ, Wurtman RJ. Metabotropic glutamate receptors regulate APP processing in hippocampal neurons and cortical astrocytes derived from fetal rats. Ann N Y Acad Sci. 1996;777:338–43. https://doi.org/10.1111/j.1749-6632.1996.tb34443.x
91. Wood PL. Lipidomics of Alzheimer's disease: current status. Alzheimers Res Ther. 2012;4:5. https://doi.org/10.1186/alzrt103
92. Chan RB, Oliveira TG, Cortes EP, Honig LS, Duff KE, Small SA, et al. Comparative lipidomic analysis of mouse and human brain with Alzheimer disease. J Biol Chem. 2012;287:2678–88. https://doi.org/10.1074/jbc.M111.274142
93. Wood PL, Medicherla S, Sheikh N, Terry B, Phillipps A, Kaye JA, et al. Targeted lipidomics of frontal cortex and plasma diacylglycerols (DAG) in mild cognitive impairment and Alzheimer's disease: validation of DAG accumulation early in the pathophysiology of Alzheimer's disease. J Alzheimers Dis. 2015;48:537–46. https://doi.org/10.3233/JAD-150336

SUPPORTING INFORMATION

Additional Supporting Information may be found online in the Supporting Information section.

TABLE S1 Identification of proteins, differentially expressed proteins, phosphosites, and differentially modulated phosphosites in the EC at stages I–II, III–IV, and V–VI of NFT pathology compared with middle-aged (MA) individuals

TABLE S2 Comparison of total dysregulated proteins and dysregulated phosphoproteins in the EC and FC

TABLE S3 Annotation of GO terms for dysregulated (phospho)proteins in the EC at different stages of NFT pathology

TABLE S4 Identification of proteins, differentially expressed proteins, phosphosites, and differentially modulated phosphosites in FC area 8 at stages I–II, III–IV, and V–VI of NFT pathology compared with middle-aged (MA) individuals

TABLE S5 Annotation of GO terms for dysregulated (phospho)proteins in the FC at different stages of NFT pathology

TABLE S6 Dysregulated synaptic proteins as revealed with SynGO showing the total number of proteins, and proteins classified according to the biological process (BP) and the cellular component (CC) in the EC and FC at different stages of NFT pathology. Duplicates are seen in both lists (BP and CC); for example, SNCB has annotation BP (synaptic vesicle endocytosis-GO:0048488) and CC (presynaptic cytosol-GO:0099523). The same protein may appear several times

How to cite this article: Ferrer I, Andrés-Benito P, Ausín K, Pamplona R, del Rio JA, Fernández-Irigoyen J, et al. Dysregulated protein phosphorylation: A determining condition in the continuum of brain aging and Alzheimer's disease. *Brain Pathology*. 2021;31:e12996. https://doi.org/10.1111/bpa.12996